Robust Analysis for Principal Component Active Control Systems

Hao Yang, Rafael M. Morales, and Matthew C. Turner

***Abstract*—Principal component active control is of great interest in recent times because of its extensive use in vibration and noise reduction applications. Existing analysis for such control systems mainly focuses on simplified representations of the closed-loop system in order to obtain robust stability conditions, but they exclude key practical considerations, such as open-loop dynamics, the periodic time-varying effects generated by the transformations between the time-domain harmonic signals and the estimation of their Fourier coefficients, multi-rate issues caused by the plant and the controller operating at different sampling rates, modelling errors and particular ways of scaling the control actions. The contribution of this work is to include all the afore-mentioned effects to provide more accurate robustness conditions, which complement existing controller tuning procedures. The robustness analysis is conducted by first exploiting the time-lifting method to reformulate the Linear-Periodic-Time-Variant part of the discrete-time system into an equivalent Linear-Time-Invariant representation. Then by using the theoretical tool of Integral Quadratic Constraints, standard forms of plant uncertainty and scaling of the control actions are incorporated. A vibration control example based on the Airbus EC-145 helicopter main rotor with on-blade actuators is included to demonstrate the benefits of the contributions. The proposed design results are benchmarked against the mixed-sensitivity $\mathcal{H}_\infty$ method, highlighting for this particular application strengths and weaknesses by each approach.**

***Index Terms*—Principal component active control, Integral Quadratic Constraints, Robust control**

I. Introduction

Active control is well known for its successful applications in a wide number of sound and vibration control problems, e.g., see [1], [2]. Such control algorithms are constructed based on the minimisation of a performance function, which quantifies the energy levels of the vibration or noise signal (called also the *error signal* in the signal processing community) and control efforts. Principal Component (PC) active control exploits the Singular Value Decomposition (SVD) of the plant steady-state behaviour at the tonal frequency to decouple the control system into modes, allowing faster operation and improved performance for the closed-loop system [3]. Being a frequency-domain-based control strategy, PC control requires Fourier coefficients of the steady-state error signal at each iteration to generate the control actions, which are also comprised of Fourier coefficients. Therefore, transformations between the Fourier coefficients and their harmonic time-domain signals are required in practical implementations. This is typically accomplished in practical implementations by including an estimation filter and a harmonic modulator. The former subsystem evaluates the Fourier coefficients of the error signal, while the latter element modulates the controller actions to produce a time-domain harmonic signal.

Most of the existing literature in this area offers, to the authors' knowledge, investigation on the performance of PC algorithms, e.g., see [4]–[8], in addition to stability results based on steady-state information *only* when the open-loop system operates at the single (tonal) frequency, see [9]–[11]. Further efforts in [9] and [10] addresses the uncertainty of the steady-state behaviour using standard robust control theory methods. More recently in [12], [13], the theory of Integral Quadratic Constraints (IQCs) [14] was exploited to obtain stability criteria under the presence of scaling of the control actions and uncertain static open-loop characteristics. It is important to highlight that all of these stability analysis efforts ignore important open-loop dynamics, which originates not only from the dynamics of the physical system, but also from estimation and modulation subsystems mentioned earlier. Such dynamics are important for any reliable analysis because they may exert a de-stabilising influence on the closed-loop. As a consequence some prior results may be too conservative and may have little practical value.

One of the latest work in this line of research is presented in [15], which incorporates the open-loop dynamics in the robust analysis in an *ad hoc* manner, by relying on standard system identification tools to capture the dynamics. This however could lead to limitations in practice due to significant dynamics still being unmodelled, especially in aerospace applications (such as helicopter vibration control), where airworthiness is of paramount importance. For this reason, the work in this manuscript enhances the existing stability conditions by obtaining an accurate dynamic representation of the open-loop behaviour with the time-lifting method [16]. More specifically, this work considers the following practical considerations: i) additional dynamics, which is generated from the plant and introduced by the use of the estimation filter; ii) periodic time-varying effects, which are originated from the harmonic modulation and the estimation process, and iii) multi-rate issues, which are caused by the plant and the controller operating at different sampling times. The resulting closed-loop system is multi-rate Linear-Periodic-Time-Variant (LPTV), and the stability analysis of such system is conducted by first applying the time-lifting method [16], which reformulates the LPTV part to an *equivalent* Linear-Time-Invariant (LTI) representation operating at the same sampling time as the controller. Once in this form, the robust stability analysis can be performed on the single-rate closed-loop system by

All the authors are with the School of Engineering, Univerisity of Leicester, University Road, Leicester, LE1 7RH, UK. E-mail: hy104@le.ac.uk; rmm23@le.ac.uk; mct6@le.ac.uk

Nomenclature

Symbol	Meaning
c	Constrained control input signal
d	Tonal disturbance signal
e	Base of natural logarithms, $e = 2.718\ldots$
e	Error signal
$\mathbf{E}(\tilde{z})$	Estimation filter transfer function matrix
$\mathbf{G}(\tilde{z})$	Plant transfer function matrix
$\mathbf{G}_0$	$\mathbf{G}(e^{\mathrm{j}\omega_0 T_s})$, i.e., plant frequency response matrix at ω_0
$\mathbf{I}$	Identity matrix of appropriate dimensions
j	Imaginary unit, $\mathrm{j} = \sqrt{-1}$
$\tilde{k}, k$	Sampling indexes associated with T_s and T_c, respectively
$\mathbf{K}(z)$	Controller transfer function matrix
l_2^a	Set of square-summable discrete-time vector signals with dimension a
l_{2e}^a	Extended space of l_2^a
m	Number of plant measured outputs
n	Number of plant control inputs
T_c, T_s	Controller and open-loop sampling times, respectively
u	Control input signal
v	Control input signal projected onto the principal component space
y	Output signal projected onto the principal component space
$\tilde{z}, z$	Complex variable associated with T_s and T_c, respectively
α, γ	Controller parameters
ω_0	Tonal frequency
$\|\mathbf{f}\|$	l_2-norm of the vector $\mathbf{f}(k)$
$\|\mathbf{H}\|$	l_2 induced norm of the operator $\mathbf{H}$
$\|\mathbf{H}\|_\infty$	$\mathcal{H}_\infty$-norm of a proper real rational transfer function matrix $\mathbf{H}(z)$
$\mathbb{C}$	Set of complex numbers
$\mathbb{R}$	Set of real numbers
$\mathbb{Z}_+$	Set of nonnegative integers
$\mathbb{RH}_\infty^{a\times b}$	Set of $a \times b$ proper real rational transfer functions with poles inside the unit circle

Subscript

$_c$	Cosine coefficients of a tonal signal
$_f$	Fourier coefficients of a tonal signal
$_p$	Phasor representation of a steady-state tonal signal
$_s$	Sine coefficients of a tonal signal

Superscript

*	Complex conjugation transpose operator
$'$	Transpose operator
$\widehat{(\,)}$	Real matrices with extended dimensions

applying the theory of IQCs to obtain accurate stability results.

The paper is structured as follows: Section II provides mathematical preliminaries and introduces the IQC approach. The tonal PC control strategy is discussed in Section III, explaining the various subsystems involved. Section IV first describes the LTI-based reformulation, where the time-lifting method is applied. Then the stability analysis is conducted for the lifted closed-loop system considering the following scenarios: linear nominal stability, constrained nominal stability, robust unconstrained stability and robust constrained stability. This section concludes with comments explaining how the robust analysis might be used to complement controller design procedures. Section V provides a simulation based on a vibration reduction control problem for the Airbus helicopter EC-145 main rotor. The open-loop system is modelled by a set of LTI dynamics operating over a number of cruise conditions between 10 and 50 kt. A unique PC controller is designed and its robustness is certified with the derived robustness condition. The performance of the PC control strategy is benchmarked with an existing mixed-sensitivity $\mathcal{H}_\infty$ controller available in the literature and discussions on their strengths and weaknesses are included. This paper concludes with some overall final remarks in Section VI.

II. PRELIMINARIES

A. Notation

The notation used throughout in this paper is summarised in the Nomenclature. We use lower-case bold variables to denote column vectors while upper-case bold variables to denote matrices or operators. For the sake of generality, we use a and b to denote the dimensions of the signals and operators in this section, while in other sections, dimensions are denoted based on the number of plant inputs and outputs, expressed as n and m, respectively. Note that the size of a real matrix $\mathbf{H} \in \mathbb{R}^{a\times b}$ is also denoted by the short-hand notation $\mathbf{H}_{a\times b}$.

Let $l_2^a(\mathbb{Z}_+)$ be the space of discrete functions $\mathbf{f} : \mathbb{Z}_+ \to \mathbb{R}^a$ with finite 2-norm:

$$\|\mathbf{f}\|^2 = \sum_{k=0}^{\infty} \mathbf{f}(k)' \mathbf{f}(k) < \infty$$

The associated extended space of $l_2^a(\mathbb{Z}_+)$ is defined as:

$$l_{2e}^a(\mathbb{Z}_+) = \{\mathbf{f} : \mathbb{Z}_+ \to \mathbb{R}^a : \|P_T \mathbf{f}\| < \infty,\ \forall T \in \mathbb{Z}_+\}$$

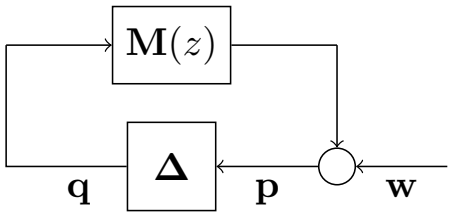

Fig. 1: Standard feedback configuration.

where P_T is the truncation operator:

$$(P_T\mathbf{f})(k) = \begin{cases} \mathbf{f}(k),\ k \leq T\ (k, T \in \mathbb{Z}_+) \\ 0,\ k > T \end{cases}$$

By an operator we mean a map $\mathbf{H} : l_{2e}^a(\mathbb{Z}_+) \rightarrow l_{2e}^b(\mathbb{Z}_+)$. The operator is bounded if

$$\|\mathbf{H}\| := \sup_{\mathbf{f}\neq 0} \frac{\|\mathbf{H}(\mathbf{f})\|}{\|\mathbf{f}\|} < \infty,\ \mathbf{f} \in l_{2e}^a(\mathbb{Z}_+)$$

If an operator is bounded on $l_{2e}^a(\mathbb{Z}_+)$, then it is also bounded on $l_2^a(\mathbb{Z}_+)$, and vice versa [17][1]. If $\mathbf{H}$ is a proper real rational transfer function matrix $\mathbf{H}(z)$ and stable (all poles are inside the complex unit circle), then the above definition gives an exact measure of highest energy gain in the system, which is also known as the $\mathcal{H}_\infty$-norm defined by:

$$\|\mathbf{H}\|_\infty = \max_\omega\ \bar{\sigma}(\mathbf{H}(e^{\mathrm{j}\omega})),\ \forall\omega \in [-\pi, \pi]$$

with $\bar{\sigma}(\mathbf{H})$ denoting the maximum singular value of the matrix $\mathbf{H}$, see [18] for more details.

B. The System for Stability Analysis

The system structure used for stability analysis in this paper is shown in Fig. 1:

$$\mathbf{p} = \mathbf{M}(z)\mathbf{q} + \mathbf{w},\ \mathbf{q} = \mathbf{\Delta}(\mathbf{p})$$

where $\mathbf{w} \in l_2^a(\mathbb{Z}_+)$. We use $\mathbf{\Delta}$ to collect the elements associated with model uncertainty and scaling of the control actions. $\mathbf{M}(z)$ denotes the LTI part of the feedback control system. It is assumed that $\mathbf{M}(z) \in \mathbb{RH}_\infty^{a\times b}$ and $\mathbf{\Delta} : l_{2e}^a(\mathbb{Z}_+) \rightarrow l_{2e}^b(\mathbb{Z}_+)$ is a bounded causal operator. It will be shown later that many stability problems can be represented in the $\mathbf{M\Delta}$-framework.

Definition (Input-Output stability): The feedback interconnection in Fig. 1 is stable if it is well-posed[2] and there exists a constant $\epsilon > 0$ such that

$$\|\mathbf{p}\| + \|\mathbf{q}\| \leq \epsilon\|\mathbf{w}\|,\ \forall\mathbf{w} \in l_2^a(\mathbb{Z}_+)$$

C. IQC Theory

The theory of IQC provides a very useful analytical stability tool for feedback systems with nonlinear and uncertain elements [14]. The framework is general and the stability results are established from input-output theory, absolute theory and robust control with both structured and unstructured uncertainties.

Let $\mathbf{\Pi} = \mathbf{\Pi}^{'} \in \mathbb{R}^{(a+b)\times(a+b)}$ be a real and symmetric matrix, known as the IQC multiplier. We say $\mathbf{\Delta}$ satisfies the IQC defined by $\mathbf{\Pi}$ (denoted also by the short-hand notation $\mathbf{\Delta} \in \mathrm{IQC}(\mathbf{\Pi})$) if [14]

$$\left\langle \begin{bmatrix} \mathbf{p} \\ \mathbf{\Delta}(\mathbf{p}) \end{bmatrix}, \mathbf{\Pi} \begin{bmatrix} \mathbf{p} \\ \mathbf{\Delta}(\mathbf{p}) \end{bmatrix} \right\rangle \geq 0,\ \forall\mathbf{p} \in l_2^a(\mathbb{Z}_+)$$

where the inner product in discrete-time is defined as

$$\langle \mathbf{p}, \mathbf{q} \rangle := \sum_{k=0}^{\infty} \mathbf{p}(k)^{'}\mathbf{q}(k) = \frac{1}{2\pi}\int_{-\pi}^{\pi} \check{\mathbf{p}}(e^{\mathrm{j}\omega})^*\check{\mathbf{q}}(e^{\mathrm{j}\omega})d\omega$$

with $\check{\mathbf{p}}(e^{\mathrm{j}\omega})$ and $\check{\mathbf{q}}(e^{\mathrm{j}\omega})$ denoting the discrete Fourier transform of the sequences $\mathbf{p}(k)$ and $\mathbf{q}(k)$, respectively.

Lemma 1 (IQC Theorem): Assume that

- $\forall\tau \in [0, 1]$, the interconnection $(\mathbf{M},\ \tau\mathbf{\Delta})$, as shown in Fig. 1, is well-posed.
- $\mathbf{\Delta} \in \mathrm{IQC}(\mathbf{\Pi})$, $\mathbf{\Pi} = \begin{bmatrix} \mathbf{\Pi}_{11} & \mathbf{\Pi}_{12} \\ \mathbf{\Pi}_{12}^{'} & \mathbf{\Pi}_{22} \end{bmatrix}$ where $\mathbf{\Pi}_{11} \geq 0$ and $\mathbf{\Pi}_{22} \leq 0$.
- $\begin{bmatrix} \mathbf{M}(e^{\mathrm{j}\omega}) \\ \mathbf{I} \end{bmatrix}^* \mathbf{\Pi} \begin{bmatrix} \mathbf{M}(e^{\mathrm{j}\omega}) \\ \mathbf{I} \end{bmatrix} < 0,\ \forall\omega \in [-\pi, \pi]$

then under the assumptions set out earlier, the system in Fig. 1 is stable.

Proof: For a detailed proof, refer to [17].

The above lemma is one specific case of the more general IQC theorem, where the set of $\mathbf{\Pi}$ can be a function of frequency, depending on the nature of $\mathbf{\Delta}$. For this work, however, it is sufficient to consider only static $\mathbf{\Pi}$.

Remark: Two specific multipliers are used in this manuscript [14]:

- Let $\mathbf{\Delta} \in \mathbb{RH}_\infty^{b\times a}$. A common way to represent modelling errors and unknown dynamics is by considering the subset such that $\|\mathbf{\Delta}\|_\infty \leq 1$. The IQC for this uncertainty can be expressed as $\mathbf{\Delta} \in \mathrm{IQC}(\mathbf{\Pi}_\Delta)$ with

$$\mathbf{\Pi}_\Delta = \begin{bmatrix} \mathbf{I} & 0 \\ 0 & -\mathbf{I} \end{bmatrix} \tag{1}$$

  The corresponding IQC theorem with the above IQC multiplier provides a particular expression of the well-known stability result known as the Small Gain theorem with unstructured uncertainty [18].
- Assume now $\mathbf{\Delta}$ is defined by multiplication with a time-varying scalar function; that is $\mathbf{q}(k) = \delta(k)\mathbf{p}(k)$, where $\delta(k) \in [-1, 1]$. In the language of IQC, $\Delta \in \mathrm{IQC}(\mathbf{\Pi}_\delta)$ with

$$\mathbf{\Pi}_\delta = \begin{bmatrix} \mathbf{X} & \mathbf{Y} \\ \mathbf{Y}^{'} & -\mathbf{X} \end{bmatrix} \tag{2}$$

  where $\mathbf{X} = \mathbf{X}^{'} \geq 0$ and $\mathbf{Y} = -\mathbf{Y}^{'}$ are real matrices. For more information, refer to [14].

[1] A similar statement follows for the definition of causality, see [17] for more details

[2] see [14] for the definition of a well-posedness.

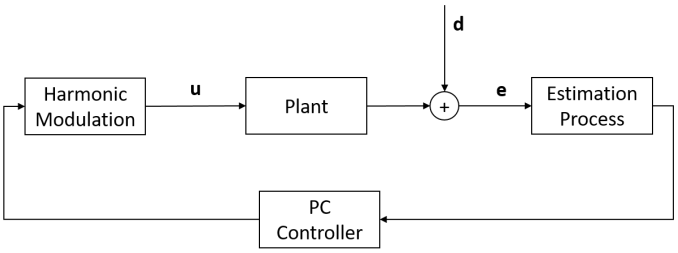

Fig. 2: General schematic of active control systems.

III. PC Active Control for Tonal Disturbances

The general diagram of PC active control systems is shown in Fig. 2, where the plant is assumed to be LTI and stable. Note that the linearity assumption is not restrictive in practical applications, a well-known example can be found in rotorcraft vibration reduction applications [19]–[24], whereby the behaviour of the main rotor is nonlinear, however, after some transformations, the relation between chosen harmonics of the input and output signals is dominantly linear.

The baseline disturbance signal ($\mathbf{d}$) represents a signal dominated by a *single* harmonic (hence the name tonal). Such disturbances are also known as deterministic (or narrowband) signals in the signal processing community, and they arise in many applications, such as rotating machinery. Fourier coefficients of these disturbances may vary slowly with time so they are often regarded as constant [9]. Tonal control strategies target this dominant harmonic disturbance and mitigate its presence. We will denote the tonal frequency by ω_0 and assume it to be constant and rational multiple of π to ensure periodicity in discrete-time [9].

Because of the linearity assumption mentioned earlier, the control input signal ($\mathbf{u}$) and the error signal ($\mathbf{e}$) are also considered to be signals dominated at the tonal frequency, where $\mathbf{u}$ has a unique and linear influence on $\mathbf{e}$. This pair forms the input and output considered for the vibration or noise reduction problem, and the performance is typically measured against $\mathbf{d}$ and expressed in terms of percentage reduction. It is worth noting that the fundamental principles of tonal control could be easily extended to multiple harmonics (multi-tonal) provided that there is no cross-coupling between the operating harmonics.

The closed-loop system in Fig. 2 operates at two different sampling rates, with the controller sampling time denoted by T_c and the rest of the system operating at a sampling time T_s. T_c is chosen much larger than T_s to make sure the estimation of the harmonic coefficients converge to accurate values. The two sampling times are typically chosen according to ω_0. In order to avoid aliasing effect, T_s is selected such that:

$$T_s = \frac{2\pi}{\zeta\omega_0},\ \zeta = 2, 3, 4, \dots$$

and to ensure that the controller updates the control actions at least one period associated with ω_0, T_c is chosen as

$$T_c = \frac{2\kappa\pi}{\omega_0},\ \kappa = 1, 2, 3 \dots$$

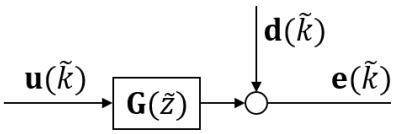

Fig. 3: Open-loop plant behaviour.

To distinguish discrete-time signals operating at these two sampling times, we introduce the following notation

$$\begin{aligned} u(\tilde{k}) &:= u(\bar{k}T_s),\ \forall \tilde{k} \in \mathbb{Z}_+ \\ u(k) &:= u(\bar{k}T_c),\ \forall k \in \mathbb{Z}_+ \end{aligned}$$

where $\bar{k} \in \mathbb{Z}_+$ is the time index. In most (if not all) practical applications, we have $T_c = T_s\beta$ where $\beta \geq 2$ is an integer. Hence every T_c seconds, $u(\tilde{k})$ is updated β times, while $u(k)$ is updated only once. The above notation is similar to those defined elsewhere, see for example [25], [26].

We also use different notation for the complex variables entering the z-transform: $\tilde{z}$ for $\tilde{k}$ and z for k, respectively. It is important to notice that $\mathbf{H}(z)$ is not equal to $\mathbf{H}(\tilde{z})$ with z replaced by $\tilde{z}$. Each of the sub-systems will be discussed in more detail as next.

A. Plant

The nominal plant behaviour is described in LTI form shown in Fig. 3, which can be represented as:

$$\mathbf{e}(\tilde{k}) = \mathbf{G}(\tilde{z})\mathbf{u}(\tilde{k}) + \mathbf{d}(\tilde{k}) \tag{3}$$

where $\mathbf{G}(\tilde{z}) \in \mathbb{RH}_\infty^{m\times n}$ represents the nominal physical plant. The error signal $\mathbf{e} : \mathbb{Z}_+ \to \mathbb{R}^m$ contains the vibration or noise signal wished to be reduced, and it is sensitive to the control input signal $\mathbf{u} : \mathbb{Z}_+ \to \mathbb{R}^n$. The baseline vibration or noise signal $\mathbf{d}(k)$ is measured in the presence of zero control input (mathematically we say $\mathbf{e} = \mathbf{d}$ when $\mathbf{u} = 0$), and it is expressed as:

$$\mathbf{d}(\tilde{k}) := \mathbf{d}_c \cos(\omega_0\tilde{k}) + \mathbf{d}_s \sin(\omega_0\tilde{k}) \tag{4}$$

where $\mathbf{d}_c \in \mathbb{R}^m$ and $\mathbf{d}_s \in \mathbb{R}^m$ vary sufficiently slow so they are considered constant in practice.

B. Harmonic Modulation

This signal processing subsystem operates every T_s seconds and modulates the Fourier coefficients provided by the control law such that:

$$\mathbf{u}(\tilde{k}) := \mathbf{u}_c(k) \cos(\omega_0\tilde{k}) + \mathbf{u}_s(k) \sin(\omega_0\tilde{k}) \tag{5}$$

where $\mathbf{u}_c(k)$ and $\mathbf{u}_s(k)$ are updated by the controller every T_c seconds, and they remain *unchanged* until the next control control iteration.

C. Estimation Process

Estimation of the harmonic coefficients of interest are required by the controller to calculate future control actions. In practical applications, the well-known heterodyne technique [27] is commonly used, and for this reason it is adopted

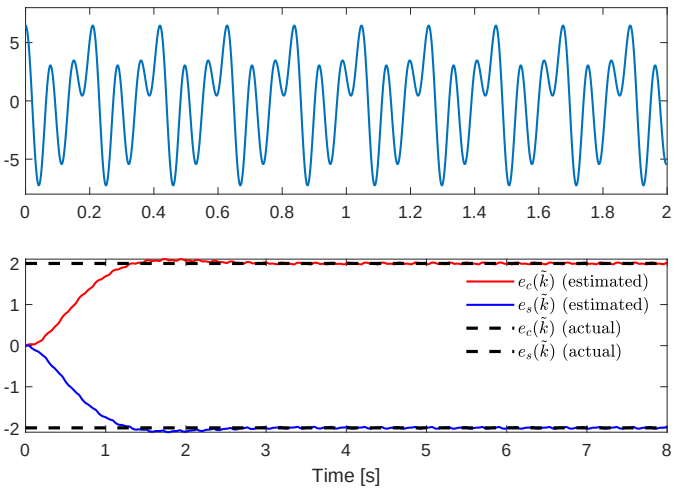

Fig. 4: Heterodyne filter behaviour.

in this work. This process operates on the following principle - say we have the following harmonic signal:

$$e(\tilde{k}) = \sum_{l=0}^{\infty} e_{cl}\cos(l\omega_0\tilde{k}) + e_{sl}\sin(l\omega_0\tilde{k})$$

A recursive estimation for the l-th harmonic coefficients of $e(\tilde{k})$ are estimated by the following expression

$$\begin{bmatrix} e_c(\tilde{k}) \\ e_s(\tilde{k}) \end{bmatrix} = 2E(\tilde{z})\mathbf{I}e(\tilde{k}) \begin{bmatrix} \cos(l\omega_0\tilde{k}) \\ \sin(l\omega_0\tilde{k}) \end{bmatrix} \tag{6}$$

where $E(\tilde{z})$ is a low-pass filter (typically Butterworth) with sampling time T_s. Fig. 4 provides an example on typical responses of a well tuned estimation filter. The upper plot illustrates the signal $e(\tilde{k})$ while the lower plot shows the time evolution for the estimation process. It is clear that the filter takes time for the estimation to be precise enough. $E(\tilde{z})$ has the mathematical property $\|E\|_\infty = 1$.

In the design of the filter, increasing the cut-off frequency leads to convergence speed improvement but accuracy degradation, and vice versa. Hence the trade-off between these two aspects should be considered according to the particular application.

D. PC Controller

PC active control strategies exploit the SVD to decouple the stady-behaviour of the plant into principal components (or singular values), which enable the designer to choose significant modes for the control task. The advantage of doing so is that control strategies based on modes with higher gain lead to lower control efforts and improved robustness properties [12]. The general PC control law is derived as follows.

Assuming that the steady-state of the system in Fig. 3 is reached in every control iteration, the k-th period can be approximated by the following complex linear relation:

$$\mathbf{e}_p(k) = \mathbf{G}_0\mathbf{u}_p(k) + \mathbf{d}_p \tag{7}$$

where $\mathbf{G}_0 = \mathbf{G}(e^{\mathrm{j}\omega_0 T_s}) \in \mathbb{C}^{m\times n}$, and we use $\mathbf{u}_p(k)$ to denote the phasor representation of the control input signal at every control iteration, i.e.,

$$\mathbf{u}_p(k) = \mathbf{u}_c(k) - \mathrm{j}\mathbf{u}_s(k)$$

Fourier coefficients of the steady-state error signal at k-th iteration are similarly collected by

$$\mathbf{e}_p(k) = \mathbf{e}_c(k) - \mathrm{j}\mathbf{e}_s(k)$$

and the constant tonal disturbance is represented by

$$\mathbf{d}_p = \mathbf{d}_c - \mathrm{j}\mathbf{d}_s$$

By applying the reduced SVD to $\mathbf{G}_0$ (assumed to have full rank), we can obtain:

$$\mathbf{G}_0 = \begin{bmatrix}\mathbf{R}_r & \mathbf{R}_\perp\end{bmatrix} \begin{bmatrix} \mathbf{\Sigma}_r & 0 \\ 0 & \mathbf{\Sigma}_\perp \end{bmatrix} \begin{bmatrix} \mathbf{Q}_r^* \\ \mathbf{Q}_\perp^* \end{bmatrix}$$

where $\mathbf{R}_r \in \mathbb{C}^{m\times r}$, $\mathbf{Q}_r \in \mathbb{C}^{n\times r}$, $\mathbf{\Sigma}_r \in \mathbb{R}^{r\times r}$ with r being the number of modes intended to control, which is chosen by the controller designer. It is clear that $r \leq \min\{m, n\}$ and $\mathbf{\Sigma}_r$ contains r largest singular values of $\mathbf{G}_0$. Also, note that $\mathbf{R}_r$ and $\mathbf{Q}_r$ have the following property:

$$\mathbf{R}_r^*\mathbf{R}_r = \mathbf{I},\ \mathbf{Q}_r^*\mathbf{Q}_r = \mathbf{I}$$

The error and input signals are captured into the modal space by the following transformations [28], [29]

$$\mathbf{v}_p(k) = \mathbf{Q}_r^*\mathbf{u}_p(k),\ \mathbf{y}_p(k) = \mathbf{R}_r^*\mathbf{e}_p(k)$$

where $\mathbf{v}_p : \mathbb{Z}_+ \to \mathbb{C}^r$ and $\mathbf{y}_p : \mathbb{Z}_+ \to \mathbb{C}^r$. Therefore, we can generalise the PC control law as

$$\mathbf{v}_p(k+1) = \mathbf{W}_v\mathbf{v}_p(k) - \mathbf{W}_y\mathbf{y}_p(k)$$

where $\mathbf{W}_v > 0 \in \mathbb{R}^{r\times r}$ is used to adjust control efforts while $\mathbf{W}_y > 0 \in \mathbb{R}^{r\times r}$ for performance. Typically, these two weight matrices are diagonal. By applying the z-transform to the above equation, the PC controller can be represented as $\mathbf{v}_p(z) = \mathbf{K}(z)\mathbf{y}_p(z)$, where

$$\mathbf{K}(z) = -(z\mathbf{I} - \mathbf{W}_v)^{-1}\mathbf{W}_y \tag{8}$$

which operates at the sampling time T_c and the dimensions of the controller are $\mathbf{K}(z) \in \mathbb{RH}_\infty^{r\times r}$.

The advantage of the representation in (8) is that well-known choices of active control algorithms can be all included under this framework [12]. In this paper, we consider the following widely used weight choices for the robustness analysis:

* **Modified steepest descent algorithm**

  $\mathbf{W}_v = \gamma\mathbf{I},\ \mathbf{W}_y = \alpha\mathbf{\Sigma}_r,$ where $\alpha > 0$ and $0 < \gamma < 1$

* **Modified Newton's algorithm**

  $\mathbf{W}_v = \gamma\mathbf{I},\ \mathbf{W}_y = \alpha\mathbf{\Sigma}_r^{-1},$ where $\alpha > 0$ and $0 < \gamma < 1$

* **Modified PC-LMS algorithm**

  $\mathbf{W}_v = \mathrm{diag}(\gamma_1, \ldots, \gamma_r),\ \mathbf{W}_y = \mathrm{diag}(\alpha_1, \ldots, \alpha_r)$

  where $\alpha_i > 0$, $0 < \gamma_i < 1$, $\forall i = 1, \ldots, r$ and diag(.) denotes the diagonal entries of a diagonal matrix.

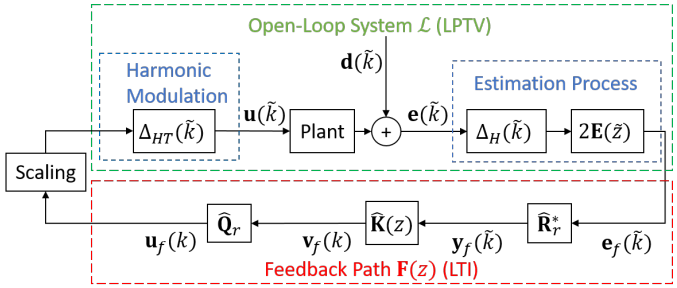

Fig. 5: Block diagram of multi-rate closed-loop PC active control in practical applications.

More information regarding weight choices in PC active control algorithms can be found in [9].

It is worth noting that for the active control to work in practice, it is preferred that T_c is much slower (larger) than the dynamics of $\mathbf{G}(\tilde{z})$ and $E(\tilde{z})$, so that accurate estimations of the harmonic coefficients of $\mathbf{e}(\tilde{k})$ are obtained, leading to better steady-state performance results generally. On the other hand, a very large T_c would imply that the control system is effectively open-loop between each control action, hence stability problems could be encountered. Consequently, the choice of T_c is of paramount importance to achieve a desired trade-off and it should be considered carefully during the design stage.

IV. Accurate Robustness Analysis

Motivated by the limitations explained in Section I of existing stability results for tonal PC control systems, whereby the open-loop dynamics are highly simplified in many situations, we proceed in this section to perform an accurate robustness analysis. The accuracy is improved by including the Linear-Time-Periodic effects of the Harmonic Modulation and Estimation Process, LTI dynamics of the plant and the filter $\mathbf{E}(\tilde{z})$, modelling errors associated with the plant, co-existing and distinct sampling times T_c and T_s and scaling of the control actions to ensure the control signal $\mathbf{u}(\tilde{k})$ fit prescribed min-max regimes, see Fig. 5.

The Fourier coefficients of $\mathbf{u}(\tilde{k})$ in (5) are collected by

$$\mathbf{u}_f(k) = \begin{bmatrix} \mathbf{u}_c(k) \\ \mathbf{u}_s(k) \end{bmatrix} = \begin{bmatrix} \mathrm{Re}(\mathbf{u}_p(k)) \\ -\mathrm{Im}(\mathbf{u}_p(k)) \end{bmatrix}$$

with $\mathbf{u}_f : \mathbb{Z}_+ \to \mathbb{R}^{2n}$. Similarly, $\mathbf{e}_f : \mathbb{Z}_+ \to \mathbb{R}^{2m}$, $\mathbf{v}_f : \mathbb{Z}_+ \to \mathbb{R}^{2r}$ and $\mathbf{y}_f : \mathbb{Z}_+ \to \mathbb{R}^{2r}$ are defined as

$$\mathbf{e}_f(\tilde{k}) = \begin{bmatrix} \mathbf{e}_c(\tilde{k}) \\ \mathbf{e}_s(\tilde{k}) \end{bmatrix}, \mathbf{v}_f(k) = \begin{bmatrix} \mathbf{v}_c(k) \\ \mathbf{v}_s(k) \end{bmatrix}, \mathbf{y}_f(k) = \begin{bmatrix} \mathbf{y}_c(k) \\ \mathbf{y}_s(k) \end{bmatrix}$$

Note that the closed-loop is represented in terms of real-valued signals. For this purpose, we use the following transformation

$$\widehat{\mathbf{Q}}_r := \begin{bmatrix} \mathrm{Re}(\mathbf{Q}_r) & \mathrm{Im}(\mathbf{Q}_r) \\ -\mathrm{Im}(\mathbf{Q}_r) & \mathrm{Re}(\mathbf{Q}_r) \end{bmatrix} \in \mathbb{R}^{2n\times 2r}$$

A similar transformation is defined for $\widehat{\mathbf{R}}_r \in \mathbb{R}^{2m\times 2r}$. Also, the controller $\mathbf{K}(z)$ is augmented such that

$$\widehat{\mathbf{K}}(z) = \begin{bmatrix} \mathbf{K}(z) & \\ & \mathbf{K}(z) \end{bmatrix} \in \mathbb{RH}_\infty^{2r\times 2r}$$

The estimation process is described by

$$\mathbf{e}_f(\tilde{k}) = 2\mathbf{E}(\tilde{z})\mathbf{\Delta}_H(\tilde{k})\mathbf{e}(\tilde{k}) \tag{9}$$

where $\mathbf{\Delta}_H : \mathbb{Z}_+ \to \mathbb{R}^{2m\times m}$ is defined as:

$$\mathbf{\Delta}_H(\tilde{k}) = \begin{bmatrix} \cos(\omega_0\tilde{k})\mathbf{I} \\ \sin(\omega_0\tilde{k})\mathbf{I} \end{bmatrix}$$

and the low-pass filter $\mathbf{E}(\tilde{z}) = E(\tilde{z})\mathbf{I} \in \mathbb{RH}_\infty^{2m\times 2m}$. Similarly, the harmonic modulation is accomplished by

$$\mathbf{u}(\tilde{k}) = \mathbf{\Delta}_{HT}(\tilde{k})\mathbf{u}_f(k) \tag{10}$$

where $\mathbf{\Delta}_{HT} : \mathbb{Z}_+ \to \mathbb{R}^{n\times 2n}$ is defined by:

$$\mathbf{\Delta}_{HT}(\tilde{k}) = \begin{bmatrix} \cos(\omega_0\tilde{k})\mathbf{I} & \sin(\omega_0\tilde{k})\mathbf{I} \end{bmatrix} \in \mathbb{R}^{n\times 2n}$$

The feedback part is collected by:

$$\mathbf{F}(z) = \widehat{\mathbf{Q}}_r\widehat{\mathbf{K}}(z)\widehat{\mathbf{R}}_r^* \in \mathbb{RH}_\infty^{2n\times 2m}$$

Overall, the *nominal* closed-loop system (without uncertainty and scaling) in Fig. 5 is a multi-rate system, where $\mathbf{F}(z)$ is LTI and generates new control input every T_c seconds, while the open-loop process is a LPTV system of period β in every control iteration and operates at T_s.

The robustness criteria presented in the next subsections are obtained by first applying the time-lifting technique, which reformulates the LPTV open-loop into an *equivalent* LTI system. More importantly, such LTI system operates at the same sampling time as the PC controller, so that a single-rate closed-loop system can be established. Then by rearranging the system into the standard $\mathbf{M\Delta}$-structure and using the Small Gain theorem [30], [31] and the theory of IQCs [14], more accurate robustness criteria will be expressed in terms of a frequency domain inequality and an equivalent Linear Matrix Inequality (LMI) result. We provide stability conditions for the following scenarios:

i) **Linear Nominal Scenario**: This analysis takes into account plant, estimation filter and controller dynamics, multi-rate sampling, and harmonic modulation. As the system in question is LTI, nominal stability is assessed purely through linear methods.

ii) **Nominal Constrained Scenario**: This analysis takes into account the same conditions as above, but with the effects of scaling the controller actions. As there are no uncertainties, but constraints, the stability must be assessed using IQC results.

iii) **Robust Unconstrained Scenario**: This analysis takes into account the same conditions as i), but including plant modelling errors, unknown dynamics or multiple operating regimes. In this case, the system is linear but uncertain and hence its robust stability can be assessed using the Small Gain Theorem.

iv) **Robust Constrained Scenario**: This analysis takes into account the same conditions as i), in addition to plant modelling errors and constraints on the controller actions. In this case, the system is nonlinear and uncertain and must, again, be assessed using the IQC techniques briefly introduced earlier.

A. Single-Rate LTI Reformulation

The time-lifting method is probably the most classical way to reformulate LPTV systems into LTI representations, where the lifting process packs the values of a signal over one period into a new signal with increased dimension [25]. As a result, the time-lifting reformulation leads to a system with enlarged size and operates at a larger sampling time, which fits well for the closed-loop system under consideration in this work. Such reformulation method is explained in detail below in terms of the nominal closed-loop system shown in Fig. 5.

Let minimal state-space representations of the nominal plant dynamics $\mathbf{G}(\tilde{z})$ and $2\mathbf{E}(\tilde{z})$ be defined as:

$$\mathbf{G}(\tilde{z}) = \mathbf{C}_G(\tilde{z}\mathbf{I} - \mathbf{A}_G)^{-1}\mathbf{B}_G + \mathbf{D}_G$$
$$2\mathbf{E}(\tilde{z}) = \mathbf{C}_E(\tilde{z}\mathbf{I} - \mathbf{A}_E)^{-1}\mathbf{B}_E + \mathbf{D}_E$$

respectively. The open-loop LPTV system $\mathcal{L}$, which relates $\mathbf{u}_f(k)$ to $\mathbf{e}_f(\tilde{k})$ can be represented as:

$$\mathcal{L} \sim \begin{cases} \mathbf{x}(\tilde{k}+1) = \mathbf{A}(\tilde{k})\mathbf{x}(\tilde{k}) + \mathbf{B}(\tilde{k})\mathbf{u}_f(k) \\ \mathbf{e}_f(\tilde{k}) = \mathbf{C}(\tilde{k})\mathbf{x}(\tilde{k}) + \mathbf{D}(\tilde{k})\mathbf{u}_f(k) \end{cases} \tag{11}$$

where

$$\mathbf{A}(\tilde{k}) = \begin{bmatrix} \mathbf{A}_G & 0 \\ \mathbf{B}_E\mathbf{\Delta}_H(\tilde{k})\mathbf{C}_G & \mathbf{A}_E \end{bmatrix},\ \mathbf{B}(\tilde{k}) = \begin{bmatrix} \mathbf{B}_G\mathbf{\Delta}_{HT}(\tilde{k}) \\ \mathbf{B}_E\mathbf{\Delta}_H(\tilde{k})\mathbf{D}_G\mathbf{\Delta}_{HT}(\tilde{k}) \end{bmatrix}$$
$$\mathbf{C}(\tilde{k}) = \begin{bmatrix} \mathbf{D}_E\mathbf{\Delta}_H(\tilde{k})\mathbf{C}_G & \mathbf{C}_E \end{bmatrix},\ \mathbf{D}(\tilde{k}) = \mathbf{D}_E\mathbf{\Delta}_H(\tilde{k})\mathbf{D}_G\mathbf{\Delta}_{HT}(\tilde{k})$$

and $\mathbf{x}(\tilde{k}) = \begin{bmatrix} \mathbf{x}_G(\tilde{k}) \\ \mathbf{x}_E(\tilde{k}) \end{bmatrix}$ with $\mathbf{x}_G(\tilde{k})$ and $\mathbf{x}_E(\tilde{k})$ being the states of $\mathbf{G}(\tilde{z})$ and $2\mathbf{E}(\tilde{z})$, respectively. By using the time-lifting technique, the system in (11) can be represented by an equivalent LTI system $\mathbf{L}(z)$ operating at T_c, whose size is $2\beta m \times 2\beta n$ [16], [25], [32] such that:

$$\mathbf{L}(z) \sim \begin{cases} \mathbf{x}_L(k+1) = \bar{\mathbf{A}}\mathbf{x}_L(k) + \bar{\mathbf{B}}\mathbf{u}_L(k) \\ \mathbf{e}_L(k) = \bar{\mathbf{C}}\mathbf{x}_L(k) + \bar{\mathbf{D}}\mathbf{u}_L(k) \end{cases} \tag{12}$$

where $\bar{\mathbf{A}} \in \mathbb{R}^{(\mu+2\tau m)\times(\mu+2\tau m)}, \bar{\mathbf{B}} \in \mathbb{R}^{(\mu+2\tau m)\times 2\beta n}, \bar{\mathbf{C}} \in \mathbb{R}^{2\beta m\times(\mu+2\tau m)}$ and $\bar{\mathbf{D}} \in \mathbb{R}^{2\beta m\times 2\beta n}$, with μ and τ being the number of states in $\mathbf{G}(\tilde{z})$ and $2\mathbf{E}(\tilde{z})$, respectively. The 4 matrices can be computed by using $\mathbf{A}(\tilde{k}), \mathbf{B}(\tilde{k}), \mathbf{C}(\tilde{k})$ and $\mathbf{D}(\tilde{k})$ at any control iteration, for simplicity we provide the algorithms in terms of the first control period where $\tilde{k} \in [0, \beta-1]$, hence:

$$\bar{\mathbf{A}} = \mathbf{A}(\beta-1)\mathbf{A}(\beta-2)\cdots\mathbf{A}(0)$$
$$\bar{\mathbf{B}} = \begin{bmatrix} \mathbf{A}(\beta-1)\cdots\mathbf{A}(1)\mathbf{B}(0) & \dots & \mathbf{A}(\beta-1)\mathbf{B}(\beta-2) & \mathbf{B}(\beta-1) \end{bmatrix}$$
$$\bar{\mathbf{C}} = \begin{bmatrix} \mathbf{C}(0) \\ \mathbf{C}(1)\mathbf{A}(0) \\ \vdots \\ \mathbf{C}(\beta-1)\mathbf{A}(\beta-2)\cdots\mathbf{A}(0) \end{bmatrix}$$
$$\bar{\mathbf{D}} = \begin{bmatrix} \bar{\mathbf{D}}_{11} & \dots & \bar{\mathbf{D}}_{1j} \\ \vdots & \ddots & \vdots \\ \bar{\mathbf{D}}_{i1} & \dots & \bar{\mathbf{D}}_{ij} \end{bmatrix},\ \forall i,j = 1,\dots,\beta$$

where $\bar{\mathbf{D}}_{ij} \in \mathbb{R}^{2m\times 2n}$ and can be obtained as follows

$$\bar{\mathbf{D}}_{ij} = \begin{cases} 0, & i < j \\ \mathbf{D}(i-1), & i = j \\ \mathbf{C}(i-1)\mathbf{B}(i-1), & i = j+1 \\ \mathbf{C}(i-1)\mathbf{A}(i-2)\cdots\mathbf{A}(j)\mathbf{B}(j-1), & i > j+1 \end{cases}$$

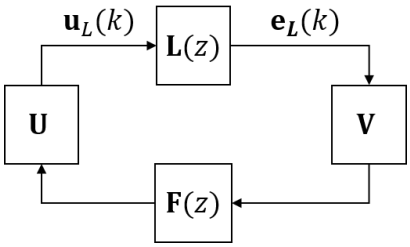

Fig. 6: Equivalent single-rate LTI representation of the nominal closed-loop system shown in Fig. 5.

It is worth noting that $\mathbf{L}(z)$ has extended dimensions and because $\mathbf{u}(k)$ is assumed constant over all the β samples in each control period, the lifted input vector $\mathbf{u}_L : \mathbb{Z}_+ \to \mathbb{R}^{2\beta n}$ is constructed by assembling β samples of $\mathbf{u}(k)$:

$$\mathbf{u}_L(k) = \begin{bmatrix} \mathbf{u}_f(k)' & \mathbf{u}_f(k)' & \dots & \mathbf{u}_f(k)' \end{bmatrix}' \tag{13}$$

which can be equivalently expressed as:

$$\mathbf{u}_L(k) = \mathbf{U}\mathbf{u}_f(k)$$

where

$$\mathbf{U} = \begin{bmatrix} \mathbf{I}_{2n\times 2n} & \mathbf{I}_{2n\times 2n} & \dots & \mathbf{I}_{2n\times 2n} \end{bmatrix}' \in \mathbb{R}^{2\beta n\times 2n}$$

Similarly the lifted output vector $\mathbf{e}_L : \mathbb{Z}_+ \to \mathbb{R}^{2\beta m}$ is defined by collecting all the output signals of the LPTV system $\mathcal{L}$ at k-th control iteration:

$$\mathbf{e}_L(k) = \begin{bmatrix} \tilde{\mathbf{e}}_f(\tilde{k})' & \tilde{\mathbf{e}}_f(\tilde{k}+1)' & \dots & \tilde{\mathbf{e}}_f(\tilde{k}+\beta-1)' \end{bmatrix}' \tag{14}$$

Since the feedback path operates at T_c, $\mathbf{e}_f(\tilde{k})$ are only processed by $\mathbf{F}(z)$ at $T_c, 2T_c, 3T_c, \dots$. These processed signals can be extracted from $\mathbf{e}_L(k)$ by using a constant matrix $\mathbf{V}$ defined as:

$$\mathbf{V} = \begin{bmatrix} \mathbf{I}_{2m\times 2m} & \mathbf{0}_{2m\times(2\beta m-2m)} \end{bmatrix} \in \mathbb{R}^{2m\times 2\beta m}$$

Therefore, the nominal closed-loop system in Fig. 5 can be equivalently described by a single-rate LTI closed-loop system as shown in Fig. 6. Since there is no simplification and dynamics missing from the LPTV system given in (11) to the time-lifted LTI representation shown in (12), $\mathbf{L}(z)$ inherits the same properties of the original LPTV system, i.e., the system in (11) is stable if and only if the lifted system in (12) is stable. This analogy can be extended to controllability, observability and more, see [25] for a detailed discussion.

Remark: The boundedness of the signals in Fig. 6 implies boundedness of the signals in Fig. 5, and vice versa, because

$$\|\mathbf{u}_L\| = \|\mathbf{u}_f\|,\ \|\mathbf{e}_L\| = \|\mathbf{e}_f\|$$

Moreover, it is important to notice that in this work the lifted system $\mathbf{L}(z) \in \mathbb{RH}_\infty^{2\beta m\times 2\beta n}$, where $\mathbf{L}(z)$ is guaranteed stable since its poles are have absolute values less than one. To see this note that the poles of $\mathbf{L}(z)$ are the eigenvalues of $\bar{A}$ and that

$$\det(\lambda\mathbf{I} - \bar{\mathbf{A}}) = 0$$

where

$$\det(\lambda\mathbf{I} - \bar{\mathbf{A}}) = \det(\lambda\mathbf{I} - \mathbf{A}_E^\beta)\det(\lambda\mathbf{I} - \mathbf{A}_G^\beta)$$

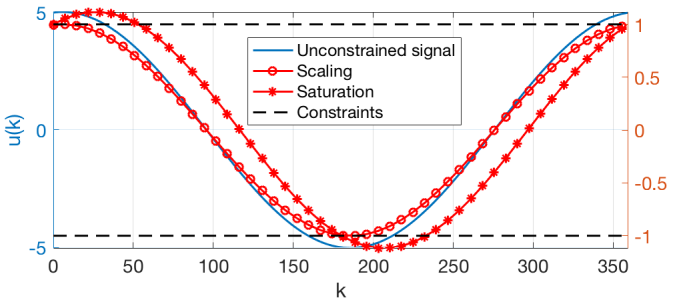

Fig. 7: Scaling vs Saturation. Scaling offer no phase shift and ensures signal fitting within min-max time-domain constraints.

B. Linear Nominal Scenario

The stability of the nominal closed-loop system, i.e., without plant uncertainty and control actions scaling, can be examined by checking the poles of the closed-loop system transfer function.

Result 1: The nominal system in Fig. 6 is stable if and only if the roots of

$$\det\left(\mathbf{I}-\mathbf{VL}(z)\mathbf{UF}(z)\right)=0$$

are within the unit circle, where $\det(.)$ denotes the determinant of a matrix.

Remark: The stability in this case is a relaxed version of the stability defined for a multi-variable LTI feedback system. However, for this result to be equivalent to the definition of *internal* stability, it is required that the closed-loop is also proper and $\mathbf{VL}(z)\mathbf{UF}(z)$ is both stabilisable and detectable. These additional conditions should not offer major restrictions when applying them on practical implementations. For more information refer to [18]. In the following stability analysis, we always assume that the closed-loop system is nominally stable.

C. Nominal Constrained Scenario

It is common in practice to restrict the control inputs in order to fit within the actuator's operating regime. Generally there are several ways to constrain a signal, such as saturation and scaling. The manuscript considers scaling only because it avoids changing the direction of the control actions. Clipping or saturating the control signals individually translates to flap signals with different phase from unconstrained actions, which then in turn could change the performance significantly [24]. This is illustrated in Fig. 7, which assumes an unconstrained harmonic control action with cosine and sine coefficients equal to 10 and 0.5, respectively. The signal is intended to be restricted in the time-domain to the range $[-1,1]$. Unlike unnormalised saturation, scaling offers no phase shift and guarantees that the signal fits within the limits more easily. The analysis with scaling instead of element-wise saturation also brings the benefit of not using frequency-dependent IQC multipliers, which facilitates the implementation of the robustness test later on.

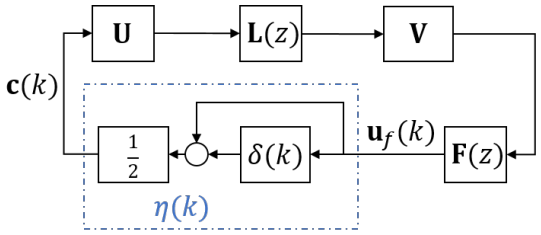

Fig. 8: Equivalent single-rate LTI system with input scaling.

Generally, the scaling is considered by a time-varying normalising factor $\eta(k)\in[0,1]$, and the constrained input signal can be expressed as:

$$\mathbf{c}(k)=\eta(k)\mathbf{u}_f(k)$$

where $\mathbf{c}(k)$ is constrained such that:

$$\sqrt{\mathbf{c}_i^2(k)+\mathbf{c}_{i+r}^2(k)}\leq 1,\ \forall i=1,\ldots,r$$

with i denoting the i-th element of $\mathbf{c}(k)$. The block diagram of the corresponding system can be represented as shown in Fig. 8, where $\eta(k)$ is transformed from $\delta(k)\in[-1,1]$ such that $\eta(k)=\frac{1}{2}(\delta(k)+1)$. This transformation is required to be compatible with the IQC and robust control analysis methods.

It is clear that the open-loop LPTV system in this case can still be captured by the lifted LTI system, i.e., $\mathbf{e}_f(k)=\mathbf{VL}(z)\mathbf{U}\mathbf{c}(k)$. Therefore, the stability of the original LPTV system subject to input scaling is equivalent to that of the system shown in Fig. 8, which can be rearranged into the standard $\mathbf{M\Delta}$-structure in Fig. 1 with $\delta(k)$ being $\mathbf{\Delta}$ and $\mathbf{M}(z)$ defined as:

$$\mathbf{M}(z)=\left(2\mathbf{I}-\mathbf{F}(z)\mathbf{VL}(z)\mathbf{U}\right)^{-1}\mathbf{F}(z)\mathbf{VL}(z)\mathbf{U}\in\mathbb{RH}_\infty^{2n\times 2n}$$

It follows from **Lemma 1** that we can obtain the following criterion.

Result 2: The system described in Fig. 8 is stable if

$$\begin{bmatrix}\mathbf{M}(e^{\mathrm{j}\omega T_c})\\ \mathbf{I}\end{bmatrix}^*\mathbf{\Pi}_\delta\begin{bmatrix}\mathbf{M}(e^{\mathrm{j}\omega T_c})\\ \mathbf{I}\end{bmatrix}<0,\ \forall\omega T_c\in[-\pi,\pi] \quad (15)$$

where $\mathbf{\Pi}_\delta$ is defined in (2).

In practice, the above frequency domain inequality is often solved as a LMI by exploiting the Kalman-Yakubovich-Popov (KYP) lemma [33].

Corollary 1: Let $\mathbf{M}(z)$ have a state-space representation

$$\mathbf{M}(z)=\mathbf{C}_\delta(z\mathbf{I}-\mathbf{A}_\delta)^{-1}\mathbf{B}_\delta+\mathbf{D}_\delta$$

with $|e^{\mathrm{j}\omega T_c}\mathbf{I}-\mathbf{A}_\delta|\neq 0$ for $\omega T_c\in[-\pi,\pi]$, $\mathbf{A}_\delta\in\mathbb{R}^{\rho\times\rho}$ and $(\mathbf{A}_\delta,\mathbf{B}_\delta)$ being a stabilisable pair. The system in Fig. 8 is stable if there exist $\mathbf{P}_\delta=\mathbf{P}_\delta^{'}\in\mathbb{R}^{\rho\times\rho}$, $\mathbf{X}=\mathbf{X}^{'}\in\mathbb{R}^{2n\times 2n}\geq 0$ and $\mathbf{Y}=-\mathbf{Y}^{'}\in\mathbb{R}^{2n\times 2n}$ such that

$$\begin{bmatrix}\mathbf{A}_\delta^{'}\mathbf{P}_\delta\mathbf{A}_\delta-\mathbf{P}_\delta & \mathbf{A}_\delta^{'}\mathbf{P}_\delta\mathbf{B}_\delta\\ \mathbf{B}_\delta^{'}\mathbf{P}_\delta\mathbf{A}_\delta & \mathbf{B}_\delta^{'}\mathbf{P}_\delta\mathbf{B}_\delta\end{bmatrix}+\mathbf{N}_\delta<0 \quad (16)$$

where

$$\mathbf{N}_\delta=\begin{bmatrix}\mathbf{C}_\delta^{'}\mathbf{X}\mathbf{C}_\delta & \mathbf{C}_\delta^{'}\mathbf{X}\mathbf{D}_\delta+\mathbf{C}_\delta^{'}\mathbf{Y}\\ \mathbf{D}_\delta^{'}\mathbf{X}\mathbf{C}_\delta+\mathbf{Y}^{'}\mathbf{C}_\delta & \mathbf{D}_\delta^{'}\mathbf{X}\mathbf{D}_\delta+\mathbf{Y}^{'}\mathbf{D}_\delta+\mathbf{D}_\delta^{'}\mathbf{Y}-\mathbf{X}\end{bmatrix}$$

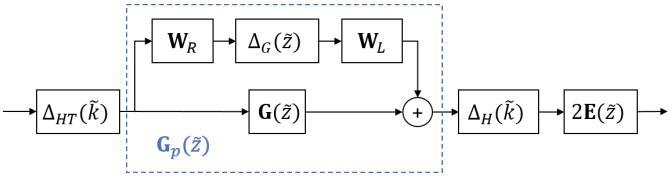

Fig. 9: Open-loop LPTV system with plant uncertainty.

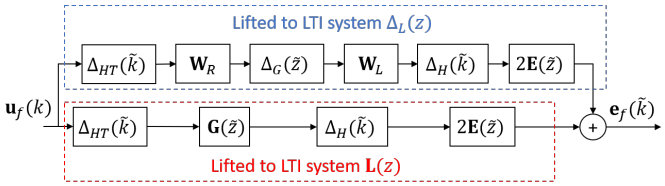

Fig. 10: Equivalent representation of Fig. 9.

The LMI implementation of the stability criterion is preferred over the frequency-domain criterion (Result 2) because modern LMI solvers can provide a solution set $\mathbf{P}$, $\mathbf{X}$ and $\mathbf{Y}$ such that the stability condition is satisfied. Note that this stability condition is only sufficient, meaning that the actual system could be stable even though the IQC condition is not satisfied.

D. Robust Unconstrained Scenario

In order to account for the modelling errors of the plant and unknown dynamics, we model the plant as shown in Fig. 9:

$$\mathbf{G}_P(\tilde{z}) = \mathbf{G}(\tilde{z}) + \mathbf{W}_L\mathbf{\Delta}_G(\tilde{z})\mathbf{W}_R \tag{17}$$

where $\mathbf{\Delta}_G(\tilde{z}) \in \mathbb{RH}_\infty^{m\times n}$ operates at T_s and it is known as unstructured uncertainty [18]. The uncertainty is normalised such that $\|\mathbf{\Delta}_G\|_\infty \leq 1$. Equation (17) can be used to represent 4 common types of uncertainties:

* **Input additive uncertainty:**

$$\mathbf{G}_P(\tilde{z}) = \mathbf{G}(\tilde{z}) + \mathbf{W}\mathbf{\Delta}_{\tilde{G}}(\tilde{z})$$

where $\mathbf{W}_L = \mathbf{W} \in \mathbb{R}^{m\times m}$ and $\mathbf{W}_R = \mathbf{I} \in \mathbb{R}^{n\times n}$ is assumed diagonal.

* **Output additive uncertainty:**

$$\mathbf{G}_P(\tilde{z}) = \mathbf{G}(\tilde{z}) + \mathbf{\Delta}_G(\tilde{z})\mathbf{W}$$

where $\mathbf{W}_L = \mathbf{I} \in \mathbb{R}^{m\times m}$ and $\mathbf{W}_R = \mathbf{W} \in \mathbb{R}^{n\times n}$ is assumed diagonal.

* **Input multiplicative uncertainty:**

$$\mathbf{G}_P(\tilde{z}) = \mathbf{G}(\tilde{z})(\mathbf{I} + \mathbf{W}\mathbf{\Delta}_G(\tilde{z}))$$

where $\mathbf{W}_L = \mathbf{G}(\tilde{z})\mathbf{W} \in \mathbb{RH}_\infty^{m\times m}$ and $\mathbf{W}_R = \mathbf{I} \in \mathbb{R}^{n\times n}$, valid for $m \geq n$.

* **Output multiplicative uncertainty:**

$$\mathbf{G}_P(\tilde{z}) = (\mathbf{I} + \mathbf{\Delta}_G(\tilde{z})\mathbf{W})\mathbf{G}(\tilde{z})$$

where $\mathbf{W}_L = \mathbf{I} \in \mathbb{R}^{m\times m}$ and $\mathbf{W}_R = \mathbf{W}\mathbf{G}(\tilde{z}) \in \mathbb{RH}_\infty^{n\times n}$, valid for $m \leq n$.

The open-loop system with plant uncertainty in Fig. 9 can be equivalently expressed in Fig. 10, where $\mathbf{\Delta}_{HT}(\tilde{k})$, $\mathbf{\Delta}_H(\tilde{k})$ and $2\mathbf{E}(\tilde{z})$ are rearranged into the uncertainty path. Therefore, it becomes also LPTV of period β samples at each control iteration and can be reformulated into an equivalent LTI system operating at T_c. Hence, the original LPTV open-loop system with plant uncertainty can be time-lifted such that:

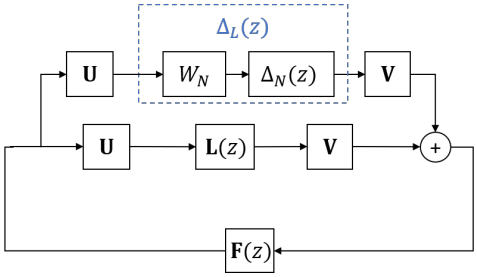

Fig. 11: Equivalent single-rate LTI system with plant uncertainty.

$$\mathbf{e}_L(k) = (\mathbf{\Delta}_L(z) + \mathbf{L}(z))\mathbf{u}_L(k)$$

where $\mathbf{L}(z)$ is defined in 12, and $\mathbf{\Delta}_L(z)$ is the lifted LTI representation of the plant uncertainty, which is bounded such that:

$$\|\mathbf{\Delta}_L\|_\infty \leq 2\|\mathbf{W}_L\|_\infty\|\mathbf{W}_R\|_\infty$$

To see this we note that because the l_2-induced norm of a LPTV system is equivalent to that of its time-lifting representation, see [34]–[36] for detailed information regarding the l_2-induced norm of LPTV systems, then:

$$\|\mathbf{\Delta}_L\| = 2\|\mathbf{E}\mathbf{\Delta}_H\mathbf{W}_L\mathbf{\Delta}_G\mathbf{W}_R\mathbf{\Delta}_{HT}\|$$

According to the sub-multiplicative property:

$$\frac{\|\mathbf{\Delta}_L\|}{2} \leq \|\mathbf{E}\|\|\mathbf{\Delta}_H\|\|\mathbf{W}_L\|\|\mathbf{\Delta}_G\|\|\mathbf{W}_R\|\|\mathbf{\Delta}_{HT}\|$$

Further notice that the l_2-induced norm of LTI systems is equivalent to the well-known $\mathcal{H}_\infty$-norm, hence:

$$\frac{\|\mathbf{\Delta}_L\|_\infty}{2} \leq \|\mathbf{E}\|_\infty\|\mathbf{\Delta}_H\|\|\mathbf{W}_L\|_\infty\|\mathbf{\Delta}_G\|_\infty\|\mathbf{W}_R\|_\infty\|\mathbf{\Delta}_{HT}\|$$

It is clear that $\|\mathbf{E}\|_\infty = \|\mathbf{\Delta}_H\| = \|\mathbf{\Delta}_{HT}\| = 1$, and with the assumption of $\|\mathbf{\Delta}_G\|_\infty \leq 1$, we obtain:

$$\|\mathbf{\Delta}_L\|_\infty \leq 2\|\mathbf{W}_L\|_\infty\|\mathbf{W}_R\|_\infty$$

Therefore, we can normalise $\|\mathbf{\Delta}_L\|_\infty$ such that:

$$\mathbf{\Delta}_L(z) = \mathbf{\Delta}_N(z)W_N$$

where $\mathbf{\Delta}_N(z)$ is the normalised lifted uncertainty defined as:

$$\|\mathbf{\Delta}_N\|_\infty \leq 1$$

with its weight W_N being a scalar and calculated by:

$$W_N = 2\|\mathbf{W}_L\|_\infty\|\mathbf{W}_R\|_\infty$$

Hence, without any loss of generality, the stability of the original LPTV system subject to unstructured plant uncertainty $\|\mathbf{\Delta}_G\|_\infty \leq 1$ in Fig. 10 is equivalent to that of the LTI system in Fig. 11 with $\|\mathbf{\Delta}_N\|_\infty \leq 1$.

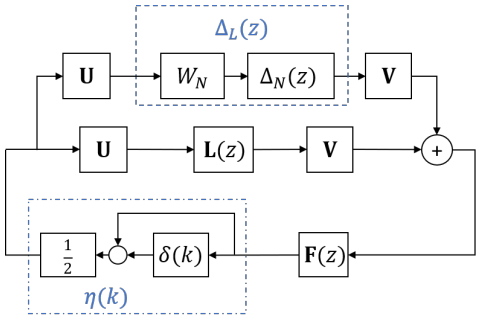

Fig. 12: Equivalent single-rate LTI system with plant uncertainty and input scaling.

Let $\mathbf{\Delta}_N(z)$ be $\mathbf{\Delta}$, we can rearrange the block diagram in Fig. 11 into the standard $\mathbf{M\Delta}$-configuration in Fig. 1, where

$$\mathbf{M}(z) = W_N\mathbf{U}\left(\mathbf{I} - \mathbf{F}(z)\mathbf{V}\mathbf{L}(z)\mathbf{U}\right)^{-1}\mathbf{F}(z)\mathbf{V} \in \mathbb{RH}_\infty^{2\beta n\times 2\beta m}$$

then we can obtain the following stability criterion.

Result 3: The system in Fig. 11 is stable for all $\mathbf{\Delta}_N(z)$ such that $\|\mathbf{\Delta}_N\|_\infty \leq 1$ if and only if [18]

$$\|\mathbf{M}\|_\infty < 1 \tag{18}$$

Remark : The above result is obtained by using the Small Gain theorem [18]. Similar result can also be achieved by exploiting the IQCs: the system described in Fig. 11 is stable if

$$\begin{bmatrix}\mathbf{M}(e^{\mathrm{j}\omega T_c})\\ \mathbf{I}\end{bmatrix}^* \mathbf{\Pi}_\Delta \begin{bmatrix}\mathbf{M}(e^{\mathrm{j}\omega T_c})\\ \mathbf{I}\end{bmatrix} < 0,\ \forall \omega T_c \in [-\pi,\pi]$$

where $\mathbf{\Pi}_\Delta$ is defined in (1).

Corollary 2: Let $\mathbf{M}(z)$ have a state-space representation

$$\mathbf{M}(z) = \mathbf{C}_\Delta(z\mathbf{I} - \mathbf{A}_\Delta)^{-1}\mathbf{B}_\Delta + \mathbf{D}_\Delta$$

with $|e^{\mathrm{j}\omega T_c}\mathbf{I} - \mathbf{A}_\Delta| \neq 0$ for $\omega T_c \in [-\pi,\pi]$, $\mathbf{A}_\Delta \in \mathbb{R}^{\xi\times\xi}$ and $(\mathbf{A}_\Delta, \mathbf{B}_\Delta)$ being a stabilisable pair. The system in Fig. 11 is stable if there exists a symmetric matrix $\mathbf{P}_\Delta \in \mathbb{R}^{\xi\times\xi}$ such that

$$\begin{bmatrix}\mathbf{A}_\Delta^{'}\mathbf{P}_\Delta\mathbf{A}_\Delta - \mathbf{P}_\Delta & \mathbf{A}_\Delta^{'}\mathbf{P}_\Delta\mathbf{B}_\Delta\\ \mathbf{B}_\Delta^{'}\mathbf{P}_\Delta\mathbf{A}_\Delta & \mathbf{B}_\Delta^{'}\mathbf{P}_\Delta\mathbf{B}_\Delta\end{bmatrix} + \mathbf{N}_\Delta < 0$$

where

$$\mathbf{N}_\Delta = \begin{bmatrix}\mathbf{C}_\Delta^{'}\mathbf{C}_\Delta & \mathbf{C}_\Delta^{'}\mathbf{D}_\Delta\\ \mathbf{D}_\Delta^{'}\mathbf{C}_\Delta & -(\mathbf{I} - \mathbf{D}_\Delta^{'}\mathbf{D}_\Delta)\end{bmatrix}$$

The advantage of using the Small Gain theorem is since $\mathbf{M}(z)$ and $\mathbf{\Delta}_N(z)$ are stable LTI systems, the result in (18) is necessary and sufficient [18], [37].

E. Robust Constrained Scenario

This final robustness condition represents the main contribution as the stability criterion includes all major practical considerations. When the system is subject to both control input scaling and plant uncertainty, the block diagram of the closed-loop PC active control system is described in Fig. 12. It follows from the previous analysis that the stability of the original LPTV system with both plant uncertainty and input scaling is equivalent to that of the system in Fig. 12, which can be captured by the $\mathbf{M\Delta}$-structure shown in Fig. 1 with

$$\mathbf{\Delta} = \begin{bmatrix}\mathbf{\Delta}_N(z) & 0\\ 0 & \delta\mathbf{I}\end{bmatrix}$$

and

$$\mathbf{M}(z) = \begin{bmatrix}\mathbf{M}_{11}(z) & \mathbf{M}_{12}(z)\\ \mathbf{M}_{21}(z) & \mathbf{M}_{22}(z)\end{bmatrix} \in \mathbb{RH}_\infty^{2(\beta n+n)\times 2(\beta m+n)}$$

where the submatrices of $\mathbf{M}(z)$ are expressed as:

$$\mathbf{M}_{11}(z) = W_N\mathbf{U}\left(2\mathbf{I} - \mathbf{F}(z)\mathbf{V}\mathbf{L}(z)\mathbf{U}\right)^{-1}\mathbf{F}(z)\mathbf{V} \in \mathbb{RH}_\infty^{2\beta n\times 2\beta m}$$
$$\mathbf{M}_{12}(z) = \frac{1}{2}W_N\mathbf{U}\left(\mathbf{I} + \mathbf{M}_{22}(z)\right) \in \mathbb{RH}_\infty^{2\beta n\times 2n}$$
$$\mathbf{M}_{21}(z) = 2\left(2\mathbf{I} - \mathbf{F}(z)\mathbf{V}\mathbf{L}(z)\mathbf{U}\right)^{-1}\mathbf{F}(z)\mathbf{V} \in \mathbb{RH}_\infty^{2n\times 2\beta m}$$
$$\mathbf{M}_{22}(z) = \left(2\mathbf{I} - \mathbf{F}(z)\mathbf{V}\mathbf{L}(z)\mathbf{U}\right)^{-1}\mathbf{F}(z)\mathbf{V}\mathbf{L}(z)\mathbf{U} \in \mathbb{RH}_\infty^{2n\times 2n}$$

then $\mathbf{\Delta} \in \mathrm{IQC}(\mathbf{\Pi}_M)$ if

$$\mathbf{\Pi}_M = \left[\begin{array}{cc|cc}\mathbf{I}_{2\beta n\times 2\beta n} & & 0 & \\ & \mathbf{X}_{2n\times 2n} & & \mathbf{Y}_{2n\times 2n}\\ \hline 0 & & -\mathbf{I}_{2\beta m\times 2\beta m} & \\ & \mathbf{Y}_{2n\times 2n}^{'} & & -\mathbf{X}_{2n\times 2n}\end{array}\right] \tag{19}$$

where $\mathbf{X}, \mathbf{Y}$ are defined in (2).

Theorem 1: The system with input scaling and uncertainty in Fig. 12 is stable if

$$\begin{bmatrix}\mathbf{M}(e^{\mathrm{j}\omega T_c})\\ \mathbf{I}\end{bmatrix}^* \mathbf{\Pi}_M \begin{bmatrix}\mathbf{M}(e^{\mathrm{j}\omega T_c})\\ \mathbf{I}\end{bmatrix} < 0,\ \forall \omega T_c \in [-\pi,\pi] \tag{20}$$

Similarly, we can also exploit the KYP lemma to perform the above stability condition as an LMI.

Corollary 3: Let $\mathbf{M}(z)$ have the state-space representation

$$\mathbf{M}(z) = \mathbf{C}_M(z\mathbf{I} - \mathbf{A}_M)^{-1}\mathbf{B}_M + \mathbf{D}_M$$

with $|e^{\mathrm{j}\omega T_c}\mathbf{I} - \mathbf{A}_M| \neq 0$ for $\omega T_c \in \begin{bmatrix}-\pi & \pi\end{bmatrix}$, $\mathbf{A}_M \in \mathbb{R}^{s\times s}$ and $(\mathbf{A}_M, \mathbf{B}_M)$ being a stabilisable pair. The system in Fig. 12 is stable if there exist symmetric matrices $\mathbf{P} \in \mathbb{R}^{s\times s}$, $\mathbf{X} = \mathbf{X}^{'} \geq 0 \in \mathbb{R}^{2n\times 2n}$ and $\mathbf{Y} = -\mathbf{Y}^{'} \in \mathbb{R}^{2n\times 2n}$ such that [33]

$$\begin{bmatrix}\mathbf{A}_M^{'}\mathbf{P}\mathbf{A}_M - \mathbf{P} & \mathbf{A}_M^{'}\mathbf{P}\mathbf{B}_M\\ \mathbf{B}_M^{'}\mathbf{P}\mathbf{A}_M & \mathbf{B}_M^{'}\mathbf{P}\mathbf{B}_M\end{bmatrix} + \mathbf{N} < 0 \tag{21}$$

where

$$\mathbf{N} = \begin{bmatrix}\mathbf{N}_{11} & \mathbf{N}_{12}\\ \mathbf{N}_{12}^{'} & \mathbf{N}_{22}\end{bmatrix}$$

and

$$\mathbf{N}_{11} = \mathbf{C}_M^{'}\begin{bmatrix}\mathbf{I} & 0\\ 0 & \mathbf{X}\end{bmatrix}\mathbf{C}_M$$
$$\mathbf{N}_{12} = \mathbf{C}_M^{'}\begin{bmatrix}0 & 0\\ 0 & \mathbf{Y}\end{bmatrix} + \mathbf{C}_M^{'}\begin{bmatrix}\mathbf{I} & 0\\ 0 & \mathbf{X}\end{bmatrix}\mathbf{D}_M$$
$$\mathbf{N}_{22} = \begin{bmatrix}-\mathbf{I} & 0\\ 0 & -\mathbf{X}\end{bmatrix} + \begin{bmatrix}0 & 0\\ 0 & \mathbf{Y}^{'}\end{bmatrix}\mathbf{D}_M + \mathbf{D}_M^{'}\begin{bmatrix}0 & 0\\ 0 & \mathbf{Y}\end{bmatrix} + \mathbf{D}_M^{'}\begin{bmatrix}\mathbf{I} & 0\\ 0 & \mathbf{X}\end{bmatrix}\mathbf{D}_M$$

Remark: Note that although the LMI implementation of the stability criterion is preferred over the frequency-domain criterion (**Theorem 1**), the efficiency of solving the LMI

in (21) depends on the size of β and the order of $\mathbf{M}(z)$, i.e., if the original LPTV system $\mathcal{L}$ is of a large period number β or $\mathbf{M}(z)$ is with high order, then the LMI condition would have a very large dimension, leading potentially to the computation becoming intractable. In such circumstances, model reduction methods can be exploited to overcome such computational complexity where the reduced-order system of $\mathbf{M}(z)$, denoted as $\mathbf{M}_R(z)$, is first used in (21) to search for a valid set of the IQC multipliers $\mathbf{X}$ and $\mathbf{Y}$. Then the obtained multipliers can be used in either (20) or (21) to verify the robust stability, see [38] for more detailed information.

F. PC Controller Design Guidance

The improved robustness results in this work support the certification of designed PC controllers tuned typically on simplified representations of the open-loop system. General guidance on the tuning procedures and the exploitation of the provided robustness conditions are provided below:

1) Examine the singular values of $\mathbf{G}_0$ according to ω_0 and determine the control modes r. Note that modes with extremely small singular values are very difficult to control, for this reason they are often ignored in the controller design. In order to obtain good vibration reduction as well as fast convergence, it is recommended to control only the modes which are not less than 10% of the largest singular value.
2) Choose one of the the control law strategies, as described in Section III-D. Note that Newtons methods is preferred to steepest-descent due to faster convergence [9]. Also, Newton's and steepest descent are preferred to PC-LMS because of fewer controller parameters to tune. If the singular values are significantly different, then the PC-LMS method is perhaps the recommended approach since closed-loop convergence and steady-state vibration reduction can be tuned for each mode separately.
3) Determine the controller parameter γ or γ_i according to control efforts. For good performance, this parameter should be selected close to 1. Also, it should be noted that γ_i in the PC-LMS control law is typically chosen in descending order ($\gamma_1 \leq \gamma_2 \leq \cdots \leq \gamma_r$) due to the hierarchy of the singular values of $\mathbf{G}_0$.
4) The controller designer may use the decoupled nominal stability results in [13] to tune α within the following ranges:
   * **Modified steepest descent algorithm:**
   $$0 < \alpha < \frac{1+\gamma}{\overline{\sigma}^2} \tag{22}$$
   * **Modified Newton's algorithm:**
   $$0 < \alpha < 1+\gamma \tag{23}$$
   * **Modified PC-LMS algorithm:**
   $$0 < \alpha_i < \frac{1+\gamma_i}{\sigma_i},\ \forall i = 1, \ldots, r \tag{24}$$
   where σ_i and $\overline{\sigma}$ denote the i-th and the maximum singular value of $\mathbf{G}_0$ respectively.

Fig. 13: Airbus EC-145 Helicopter Demonstrator [39].

   Note that the above stability conditions are obtained under *significant simplified assumption* of a static open-loop behaviour. For this reason, **Result 1** should be used to guarantee the nominal stability of the closed-loop system.
   As mentioned earlier, α is known as the convergence coefficient (or step-size in the optimisation community). In the tuning of α, once the control efforts γ is determined, typically increasing α within the range could improve the convergence speed as well as provide better error reduction. On the other hand, large step-sizes can lead to **Result 1** not being satisfied, hence the designer should balance between pursuing performance and guaranteeing nominal stability in the tuning process during this first tuning cycle.
5) In order to proceed towards the *certification* of the control law against plant uncertainty and/or scaling of control actions, the improved stability criteria in this work (**Result 2 or 3 or Theorem 1**) may be used.
6) If the improved robustness conditions are not satisfied, then go back to step 3 to increase γ or step 4 to decrease α. Repeat until a desired level of robustness is certified, if required. Note that decreasing α will certainly compromise the performance in terms of error reduction, while increasing γ can lead to large control actions, thus how to retune these two parameters depends on the specific application.

V. On-Blade Control Example

In this section, we apply the robust PC control strategy on a rotorcraft vibration reduction problem based on a set of linear models of the Airbus EC-145 helicopter (Fig. 13) main rotor with active flaps. We exploit the main robustness result and controller design guidelines to design a *single* controller covering the flight envelope between 10 and 50 kt cruise speeds while achieving very good vibration reduction. In the design we incorporate scaling of the control actions to restrict the flap deflections of the control surfaces within 3 degrees, which are typical for this application.

A. Open-loop system

New rotorcraft technologies explore the use of On-Blade active flap mechanisms for the benefit of improved vibration reduction, leading to improved comfort and airworthiness and reduced maintenance costs. A nonlinear model of the main helicopter rotor with active control surfaces is implemented

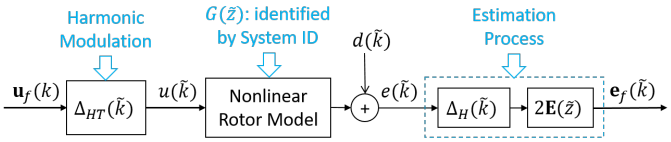

Fig. 14: Linearisation diagram.

by using the earomechanics equations described by the work of Maurice and coworkers [39]. This model has been validated against the Comprehensive Analytical Model of Rotorcraft Aerodynamics and Dynamics (CAMRAD) II [40] software and flight campaign data. Later on, the model was adapted to include rotor hub loads and implemented in MATLAB and Simulink by Alotaibi & Morales [41]. More details associated with the rotor characteristics and its aeromechanics can be found in [39], [41]. A key property of active vibration control methods for this application is that it does not interfere with the primary flight control of the vehicle.

For this particular application, we aim to reduce the vibration on the rotor *thrust* signal, which is the result of rotating vertical shear forces in the blade transmitted to the rotor hub. The control signal in this case is provided by active Trailing Edge Flap (TEF) mechanisms mounted on each blade of the main rotor, offering specific deflection angles, see Fig. 13. It follows from rotor vibration theory [42] that we target the vibration reduction efforts on the 4/rev frequency component because of the number of blades in the rotor, where the jargon 4/rev corresponds to the frequency $\omega_0 = 4\Omega$, with $\Omega = 2\pi \times 6.39$ rad/s being the rotor speed, which is maintained constant at all flight conditions.

Initial spectrum investigations on the EC-145 rotor [43] show that the relationship between the trailing edge flaps and the thrust at 4/rev is largely linear for sufficiently small flap amplitudes. Therefore, the first step of the controller design task is to obtain a LTI representation describing the vibration behaviour. This manuscript adopts the linearisation approach from [44], which offers very good validation between the nonlinear analytical rotor model and the linearised models. The linearisation approach is illustrated in Fig. 14, where in order to facilitate the controller design, the system identification is performed with a sampling time

$$T_s = \frac{2\pi}{120\Omega} \approx 0.0013 \text{ s}$$

equivalent to 3 deg azimuth position.

By using MATLAB System Identification Toolbox, linear relation described in (3) can be established in the EC-145 rotor, where the input signal $u(\tilde{k})$ corresponds to the flap deflection angle (in rad) on the *reference blade* (flap signals on the other blades are derived from those on the reference blade), the error signal $e(\tilde{k})$ accounts for the thrust vibration (in N), $d(\tilde{k})$ represents the baseline vibration obtained in the presence of zero flap and $G(\tilde{z})$ represents the linearised rotor vibration behaviour. Because both the rotor thrust and the flap signal are scalar, $G(\tilde{z})$ is identified as a discrete time 5-th order Single-Input-Single-Output (SISO) system. The harmonic modulation subsystem is required to reconstruct $\mathbf{u}_f(k)$ into $u(\tilde{k})$, as shown

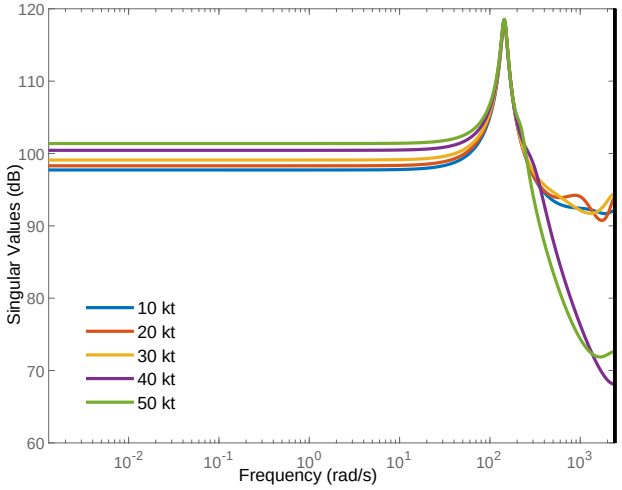

Fig. 15: Frequency responses of the identified models.

in (10). The Estimation Process has the purpose to estimate the 4/rev harmonic coefficients of $e(\tilde{k})$ provided by $\mathbf{e}_f(\tilde{k})$, as described in (9).

B. Uncertainty Modelling

The system identification is carried out at 5 different cruise speeds (10, 20, 30, 40 and 50 kt). The frequency responses of the 5 linearised systems can be observed in Fig. 15. From this frequency response we observe the rotor behaviour exhibit a noticeable change in terms of its DC gains, but reaching similar peak gain values around ω_0. At high frequencies, the behaviours differ even more, where additional modes are observed.

As mentioned earlier, we aim to design a single PC controller operating at all flight conditions. Thus, one linearised model is chosen as the nominal system while the other four systems are considered as plant uncertainty to represent the change in the flight conditions. The perturbed plant $G_P(\tilde{z})$ is described by the input multiplicative uncertainty defined in (17), where the nominal plant $G(\tilde{z})$ is the linearised system at 20 kt which has the state-space representation $G(\tilde{z}) \sim (\mathbf{A}, \mathbf{B}, \mathbf{C}, 0)$ such that:

$$\mathbf{A} = \begin{bmatrix} 1.663 & -0.5044 & -0.3231 & 0.2862 & -0.3503 \\ 1 & 0 & 0 & 0 & 0 \\ 0 & 1 & 0 & 0 & 0 \\ 0 & 0 & 1 & 0 & 0 \\ 0 & 0 & 0 & 0.5 & 0 \end{bmatrix}$$

$$\mathbf{B} = \begin{bmatrix} 512 \\ 0 \\ 0 \\ 0 \\ 0 \end{bmatrix}, \mathbf{C} = \begin{bmatrix} 69.79 & -137.4 & 40.08 & 18.97 & 0 \end{bmatrix}$$

Standard uncertainty weight modelling methods follow from fitting upper bounds of the relative errors, see Fig. 16:

$$\frac{|G_p(e^{j\omega T_s}) - G(e^{j\omega T_s})|}{|G(e^{j\omega T_s})|} \leq |W(e^{j\omega T_s})|, \ \forall \omega T_s \in [-\pi, \pi]$$

$$W(\tilde{z}) \approx \frac{0.76\tilde{z}^9 - 6.41\tilde{z}^8 + 24.12\tilde{z}^7 - 53.3\tilde{z}^6 + 76.17\tilde{z}^5 - 73\tilde{z}^4 + 46.93\tilde{z}^3 - 19.51\tilde{z}^2 + 4.76\tilde{z} - 0.52}{\tilde{z}^9 - 8\tilde{z}^8 + 28.63\tilde{z}^7 - 60.12\tilde{z}^6 + 81.67\tilde{z}^5 - 74.45\tilde{z}^4 + 45.54\tilde{z}^3 - 18.03\tilde{z}^2 + 4.2\tilde{z} - 0.44} \tag{25}$$

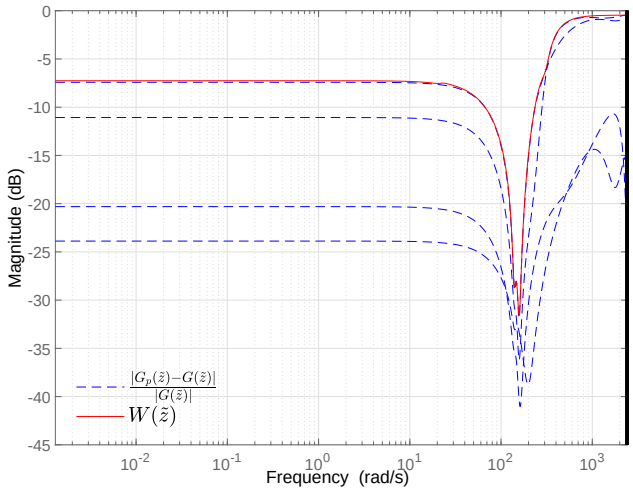

Fig. 16: Dynamic weight function.

The fitting of the uncertainty weight is performed through the command *ucover* in the Robust Control Toolbox provided by MATLAB, and a 9-th order transfer function (25). Note that the coefficients in (25) are rounded to 2 decimal places.

C. Controller Design

The controller is designed by following the steps provided in Section IV-F, where the modified PC-LMS algorithm is adopted. The controller's sampling time was chosen to operate at every tonal period

$$T_c = \frac{2\pi}{4\Omega} \approx 0.0391 \text{ s}$$

yielding a value of $\beta = 30$.

We started with $\gamma = 0.9$ and tuned α within the stability range provided by (24). By satisfying the nominal stability (**Result 1**), initial tuning values provided about 60% or so vibration reduction in nominal conditions, which was not satisfactory. Therefore, we proceeded to increase control efforts such that

$$\gamma = 0.986$$

and further adjusted α within the range

$$0 < \alpha < 4.5204 \times 10^{-6}$$

After several iterations, the following controller were finally chosen

$$\widehat{\mathbf{K}}(z) = -9.719 \times 10^{-8} \begin{bmatrix} \frac{1}{z-0.986} & 0 \\ 0 & \frac{1}{z-0.986} \end{bmatrix}$$

This control law offer about 75% vibration reduction without plant uncertainty and input scaling. The nominal closed-loop system is guaranteed stable by examining **Result 1**.

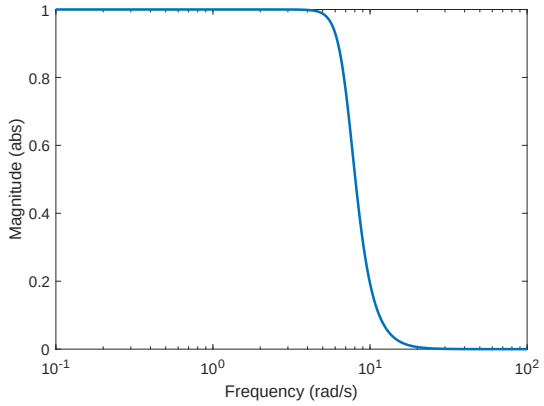

Fig. 17: Estimation filter.

D. Robustness Certification

We proceed to examine first the controller's robustness against the changing operating condition associated with different cruise speed values. The estimation filter used in the simulation is shown in Fig. 17, which is a 5th-order low-pass Butterworth filter. It follows that we first time-lift the open-loop system into $\mathbf{L}(z)$, then by applying **Result 3**, the $\mathcal{H}_\infty$-norm of $\mathbf{M}(z)$ is calculated as

$$\|\mathbf{M}\|_\infty = 0.9805$$

meaning that the controller is able to robustly stabilise the behaviour across all considered flight conditions.

We then certify the controller also against the effects of scaling the control actions by implementing **Corollary 3**. It should be noted that the input signal (flap signal) in this application is expressed in rad, and we intend to limit it within in $\pm 3^\circ$, hence the scaling factor $\eta(k)$ is multiplied by a constant gain $\frac{\pi}{60}$. As a result, the four submatrices of $\mathbf{M}(z)$ are modified accordingly:

$$\mathbf{M}_{11}(z) = W_N \mathbf{U} \left(\frac{120}{\pi} \mathbf{I} - \mathbf{F}(z)\mathbf{V}\mathbf{L}(z)\mathbf{U} \right)^{-1} \mathbf{F}(z)\mathbf{V} \in \mathbb{RH}_\infty^{60\times 60}$$

$$\mathbf{M}_{12}(z) = \frac{\pi}{120} W_N \mathbf{U} \left(\mathbf{I} + \mathbf{M}_{22}(z) \right) \in \mathbb{RH}_\infty^{60\times 2}$$

$$\mathbf{M}_{21}(z) = \frac{120}{\pi} \left(\frac{120}{\pi} \mathbf{I} - \mathbf{F}(z)\mathbf{V}\mathbf{L}(z)\mathbf{U} \right)^{-1} \mathbf{F}(z)\mathbf{V} \in \mathbb{RH}_\infty^{2\times 60}$$

$$\mathbf{M}_{22}(z) = \left(\frac{120}{\pi} \mathbf{I} - \mathbf{F}(z)\mathbf{V}\mathbf{L}(z)\mathbf{U} \right)^{-1} \mathbf{F}(z)\mathbf{V}\mathbf{L}(z)\mathbf{U} \in \mathbb{RH}_\infty^{2\times 2}$$

The LMI-based IQC condition (21) was implemented with CVX in MATLAB [45] and its solution provided the following IQC multipliers

$$\mathbf{X} = 10^9 \begin{bmatrix} 4.4238 & 0 \\ 0 & 4.4238 \end{bmatrix}, \mathbf{Y} = 0$$

Such solution was verified by implementing the frequency-domain condition in **Theorem 1** with the corresponding multiplier in (19).

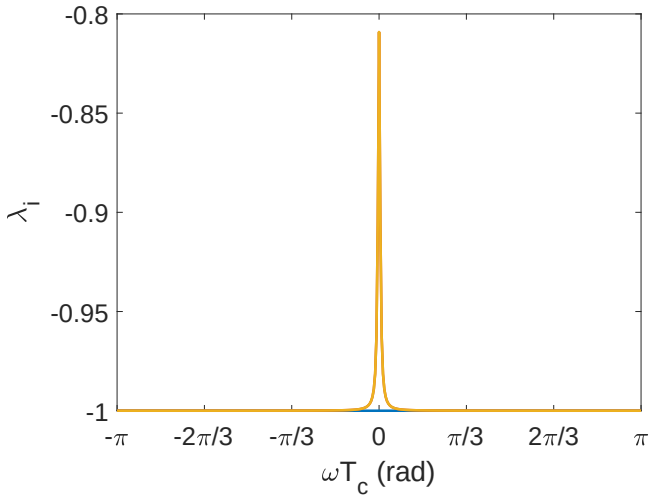

Fig. 18: IQC criterion (zoomed in).

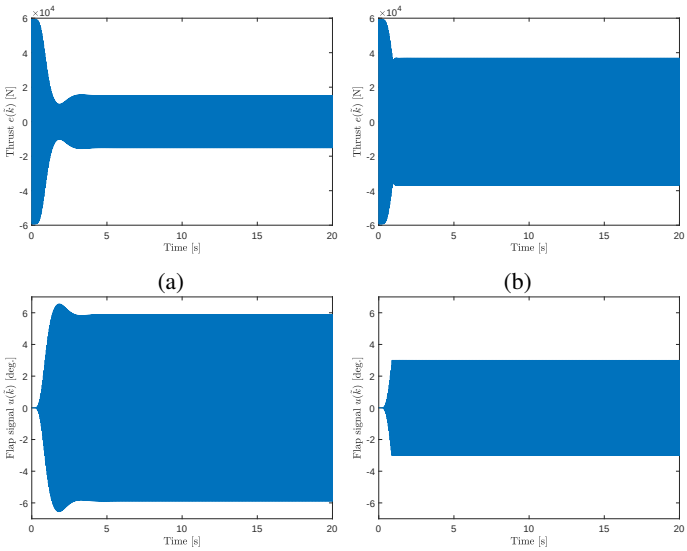

Fig. 19: Simulation results. (a) Thrust vibration (without scaling); (b) Thrust vibration (with scaling); (c) Flap signal (without scaling); (d) Flap signal (with scaling).

Relevant eigenvalues are shown Fig. 18, showing that they are negative for all frequencies. This result thus certifies the robustness of the control system against the identified cruise conditions and scaling of control actions, building increased confidence for real implementations.

E. Performance Results

1) PC Controller Performance: Simulation results are shown first for the linearised system at 20 kt. The first set of results are presented in the left column in Fig. 19, where a sufficiently large baseline disturbance is introduced and the scaling factor is *disabled*. It is clear that the controller achieves more than 70% vibration reduction but the flap angles exceeds the 3-degree limit.

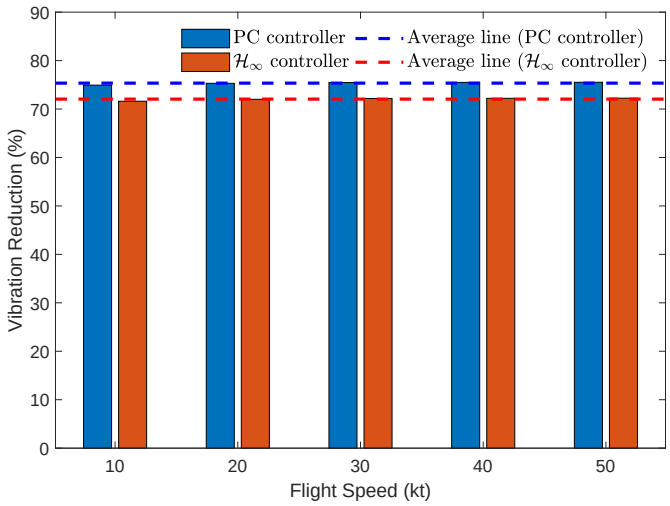

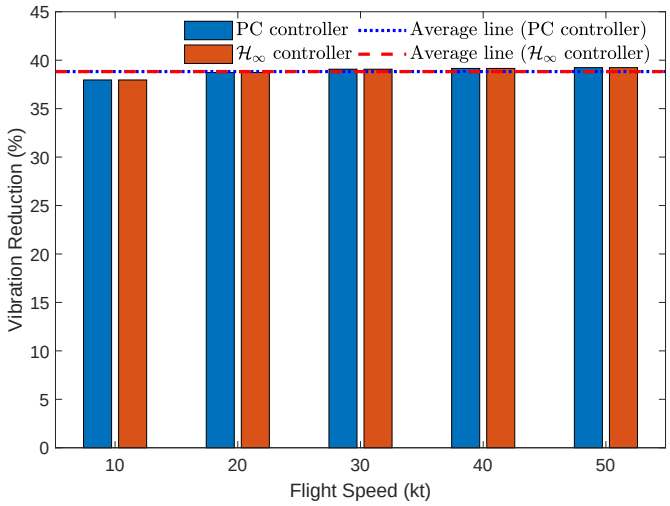

Fig. 20: Performance comparison against $\mathcal{H}_\infty$ methods. (a) Without scaling; (b) With scaling.

We then *enable* the scaling factor to observe the performance degradation, with the results shown in the right column of Fig. 19. We observe that the performance in terms of vibration reduction drops to below 40%, but the flap angles are limited to $\pm 3^\circ$. Overall in both scenarios, the PC controller shows reliability in maintaining stable operation and reaches the steady-state behaviour relatively fast (in less than 10 seconds).

2) Comparison against $\mathcal{H}_\infty$ Method: In order to show the benefits of the proposed control strategy, we compare the system performance against alternative and popular advanced controller design methods, such as Mixed-Sensitivity $\mathcal{H}_\infty$ [18]. We implement the same $\mathcal{H}_\infty$ controller available in [44], which is 17-th order and designed by shaping both the Sensitivity of the closed-loop and the transfer function associated with control actions, refer to [44] for further details. The controller is implemented in discrete form but with the smaller sampling time T_s.

The performance between the control approaches is carried

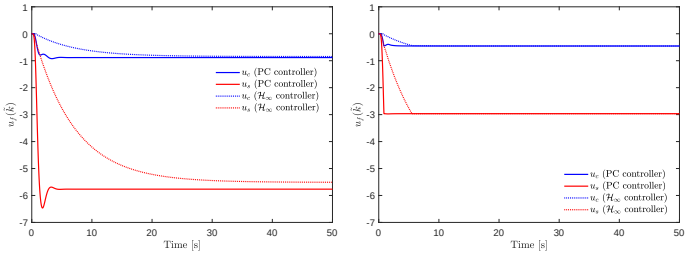

(a) (b)

Fig. 21: Control actions comparison at 20 kt. (a) Without scaling; (b) With scaling.

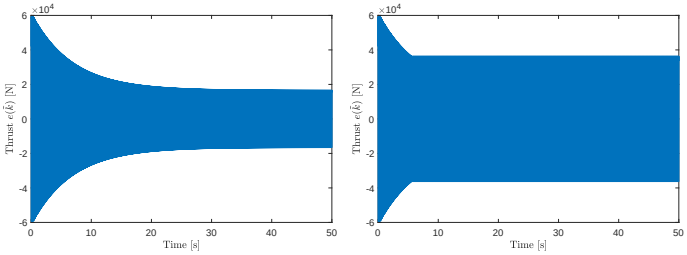

(a) (b)

Fig. 22: Thrust vibration reduction at 20 kt by using the $\mathcal{H}_\infty$ controller. (a) Without scaling; (b) With scaling.

out for two scenarios: with and without input scaling. In both cases, we test the system's performance at *each* considered flight speed, and steady-state vibration reduction results are summarised in Fig. 20. It is clear from the upper plot that when the input scaling is disabled, the PC controller provides 75% vibration reduction in average, performing slightly better than the $\mathcal{H}_\infty$ controller by 3% or so.

When the scaling factor is enabled, it is interesting to observe that both controllers offer almost the same level of vibration reduction, with the average lines being nearly 40%. This is due to the fact that both controllers converge to the same steady-state control actions, see Fig. 21. The left plot shows the control actions of both controllers operating at 20 kt when the scaling factor is not activated, and the right figure describes the control signals at the same flight speed when the scaling factor is enabled. On the other hand, the transient characteristics are rather different, with the PC controller offering much faster convergence than the $\mathcal{H}_\infty$ controller. Due to the smaller sampling time implementation of the $\mathcal{H}_\infty$, the convergence of the thrust signal is smoother than the PC controller, see Fig. 22.

F. Final Remarks on this Application

Further comments between the two control design approaches are birefly provided below, but a more detailed discussion can be found in [44]:

- Controller tuning and design efforts: The design of the PC controller is more intuitive but perhaps more time-consuming since the controller parameters are adjusted manually to balance performance, convergence speed and robustness. On the other hand, $\mathcal{H}_\infty$ control synthesis requires perhaps less tuning efforts.
- Controller implementation: The PC control strategy requires less processing power because the controller is first order and operates at a much slower sampling rate. On the contrary, the $\mathcal{H}_\infty$ controller is typically high order and operates at the smaller sampling time T_s, demanding more processing power, which could be restrictive in real applications. Order reduction methods could be implemented on the $\mathcal{H}_\infty$ controller provided that the performance is not too compromised.
- Robustness properties: One advantage of the PC control method is that accurate robustness criteria provided in this work are available. Although standard robustness conditions are also available for the $\mathcal{H}_\infty$ method including plant uncertainty, they are still more conservative than the results presented in this work because they do not include the effects of scaling the control actions [43].

In this numerical example, the simulation is conducted *only* on the linearised models of the rotor vibration behaviour to validate robust the stability results and design approach presented in this work. More comprehensive simulation results performed on the original nonlinear model is presented in [44], where a wider flight envelope is considered from 20 to 100 kt. On the other hand, because of the smaller flight envelope in this work, we are able to obtain a tighter uncertainty description, while in [44] a static uncertainty weight was required to certify the PC control law.

The current control design and assessment work is by no means complete and there are additional important practical considerations that should be taken into account, refer to [44] for more details. However, we strongly believe the principles of the control approach in this manuscript could be adapted in more general practical situations and hopefully provide the benefits in terms of improved performance and reliability.

VI. Conclusions

In this paper, an improved robust analysis for PC active control systems is conducted by including the following highly relevant practical considerations: coexisting sampling times, harmonic modulations, estimation filters, plant uncertainty and scaling of the control actions. The robustness stability criteria obtained in this work are more accurate than those available in the literature, hence increasing its practical value, especially in applications where reliability is of paramount importance such as those in rotorcraft systems. The manuscript provides also controller design recommendations, which exploit the improved robustness conditions. The results are applied to a vibration reduction application in rotorcraft and compared against more popular design methods such as $\mathcal{H}_\infty$. The case study shows that the ideas in this manuscript are successful in the sense that a controller which provides very good levels of performance can be designed and also certified for increased confidence in practical applications.

REFERENCES

[1] J. T. Pearson and R. M. Goodall, "Adaptive schemes for the active control of helicopter structural response," *IEEE Transactions on Control Systems Technology*, vol. 2, no. 2, pp. 61–72, June 1994.

[2] S. M. Kuo and S. Mitra, "Active noise control system for headphone applications," *IEEE Transactions on Control Systems Technology*, vol. 14, no. 2, pp. 331–335, March 2006.

[3] R. H. Cabell, "A principle component algorithm for feedforward active noise and vibration control," Ph.D. dissertation, Virgina Tech., 1998.

[4] R. Cabell, D. Palumbo, and J. Vipperman, "A principal component feedforward algorithm for active noise control: flight test results," *IEEE Transactions on Control Systems Technology*, vol. 9, no. 1, pp. 76–83, Jan 2001.

[5] A. Montazeri and J. Poshtan, "A new adaptive recursive RLS-based fast-array IIR filter for active noise and vibration control systems," *Signal Processing*, vol. 91, no. 1, pp. 98 – 113, 2011.

[6] Y. Xiao, "A new efficient narrowband active noise control system and its performance analysis," *IEEE Transactions on Audio, Speech, and Language Processing*, vol. 19, no. 7, pp. 1865–1874, 2011.

[7] J. Chandrasekar, L. Liu, D. Patt, P. P. Friedmann, and D. S. Bernstein, "Adaptive harmonic steady-state control for disturbance rejection," *IEEE Transactions on Control Systems Technology*, vol. 14, no. 6, pp. 993–1007, Nov 2006.

[8] R. M. Reddy, I. M. S. Panahi, and R. Briggs, "Hybrid FxRLS-FxNLMS adaptive algorithm for active noise control in fMRI application," *IEEE Transactions on Control Systems Technology*, vol. 19, no. 2, pp. 474–480, March 2011.

[9] S. J. Elliott, *Signal Processing for Active Control*. Academic Press, 2001.

[10] P. De Fonseca, P. Sas, and H. Brussel, "Robust design and robust stability analysis of active noise control systems," *Journal of Sound and Vibration*, vol. 243, pp. 23–42, 05 2001.

[11] Y. Hayakawa, A. Nakashima, T. Yasuda, and H. Ichkawa, "A new adaptive algorithm for periodic noise control and its stability analysis," *IFAC Proceedings Volumes*, vol. 47, no. 3, pp. 12 086 – 12 091, 2014, 19th IFAC World Congress.

[12] R. M. Morales and H. Yang, "Robust analysis of principal components active control via IQCs," Buenos Aires, Argentina, 2016, Multi-Conference on Systems and Control.

[13] H. Yang and R. M. Morales, "Decoupled controller tuning for robust principal component active control," Gold Coast, Australia, 2017, asian Control Conference 2017.

[14] A. Megretski and A. Rantzer, "System analysis via Integral Quadratic Constraints," *IEEE Transactions on Automatic Control*, vol. 42, no. 6, pp. 819–830, 1997.

[15] H. Yang and R. M. Morales, "Robust analysis of tonal active control systems with control scaling and estimation uncertainty," in *Proceedings of the United Kingdom Automatic Control Council (UKACC) Conference on Control*, Sheffield, UK, 2018.

[16] R. Meyer and C. Burrus, "A unified analysis of multirate and periodically time-varying digital filters," *IEEE Transactions on Circuits and Systems*, vol. 22, no. 3, pp. 162–168, 1975.

[17] U. Jönsson, "Lecture notes on Integral Quadratic Constraints," 2000, Department of Mathematics, KTH, Stockholm. ISBN 1401-2294, available at http://www.math.kth.se/~uj/.

[18] S. Skogestad and I. Postlethwaite, *Multivariable Feedback Control: Analysis and Design (Second Edition)*. John Wiley & Sons, 2005.

[19] C. Kessler, "Active rotor control for helicopters: motivation and survey on higher harmonic control," *CEAS Aeronautical Journal*, vol. 1, no. 1-4, pp. 23–54, 2011.

[20] R. M. Morales and M. C. Turner, "Robust anti-windup design for active trailing edge flaps in active rotor applications," in *Proceedings of the 70th American Helicopter Society Forum*, Montreal, Canada, 2014.

[21] R. M. Morales, M. C. Turner, P. Court, R. Hilditch, and I. Postlethwaite, "Force control of semi-active lag dampers for vibration reduction in helicopters," *IET Journal of Control Theory and Applications*, vol. 8, no. 6, pp. 409–419, 2014.

[22] R. M. Morales, M. C. Turner, P. Court, and C. Hutchin, "Actuator constraints handling in higher harmonic control algorithms for vibration reduction," in *Proceedings of the 40th European Rotorcraft Forum*, Southampton, UK, 2014.

[23] R. M. Morales, "FXLMS vs principal components in On-Blade control applications," in *Proceedings of the 42nd European Rotorcraft Forum*, Lille, France, 2016.

[24] ——, "Alternative representations of frequency domain constraints for improved performance in On-Blade control systems," in *Proceedings of European Control Conference*, Aalborg, Denmark, 2016.

[25] S. Bittanti and P. Colaneri, "Invariant representations of discrete-time periodic systems," *Automatica*, vol. 36, no. 12, pp. 1777 – 1793, 2000.

[26] G. Kranc, "Input-output analysis of multirate feedback systems," *IRE Transactions on Automatic Control*, vol. 3, no. 1, pp. 21–28, 1957.

[27] K. E. Nelson and M. A. Soderstrand, "Adaptive Heterodyne Filters (AHF) for detection and attenuation of narrow band signals," in *Acoustics, Speech and Signal Processing, 1998. Proceedings of the 1998 IEEE International Conference on*, vol. 1, 1998, pp. 441–444 vol.1.

[28] R. L. Clark, "Adaptive forward modal space control," *Journal of the Acoustic Society of America*, vol. 98, pp. 2639–2650, 1995.

[29] D. R. Morgan, "A hierarchy of performance analysis techniques for adaptive active control of sound and vibration," *The Journal of the Acoustical Society of America*, vol. 89, no. 5, pp. 2362–2369, 1991.

[30] G. Zames, "On the input-output stability of linear time-varying feedback systems - Part I: Conditions derived using concepts of loop gain, conicity and positivity," *IEEE Transactions on Automatic Control*, vol. 11, pp. 228 – 238, 1966.

[31] C. A. Desoer and M. Vidyasagar, *Feedback Systems: Input-Output Properties*. Academic Press, 1975.

[32] P. Colaneri, R. Celi, and S. Bittanti, "Constant-coefficient representations of periodic-coefficient discrete linear systems," *Journal of the American Helicopter Society*, 2004.

[33] A. Rantzer, "On the Kalman-Yakubovich-Popov lemma," *Systems and Control Letters*, vol. 28, pp. 7–10, 1996.

[34] J. Nie, R. Conway, and R. Horowitz, "Optimal $\mathcal{H}_\infty$ control for linear periodically time-varying systems in hard disk drives," *IEEE/ASME Transactions on Mechatronics*, vol. 18, no. 1, pp. 212–220, 2013.

[35] M. A. Peters and P. A. Iglesias, *Minimum Entropy Control for Time-Varying Systems*. Secaucus, NJ, USA: Birkhauser Boston, Inc., 1996.

[36] S. Mirabbasi and B. Francis, "Input-output gains of linear periodic discrete-time systems with application to multirate signal processing," in *1996 IEEE International Symposium on Circuits and Systems. Circuits and Systems Connecting the World. ISCAS 96*, vol. 2, 1996, pp. 193–196 vol.2.

[37] D. Gu, P. Petkov, and M. Konstantinov, *Robust Control Design with MATLAB*, 2005.

[38] H. Yang, R. M. Morales, and M. C. Turner, "Robust principal component algorithms for high-order fast-sampled systems," in *Proceedings of the 17th European Control Conference*, Naples, Italy, 2019.

[39] J. B. Maurice, F. A. King, and W. Fichter, "Derivation and validation of a helicopter rotor model with trailing-edge flaps," *Journal of Guidance, Control, and Dynamics*, vol. 36, no. 5, pp. 1375–1387, 2013.

[40] W. Johnson, "Technology drivers in the development of CAMRAD II," in *Proceedings of the American Helicopter Society Aeromechanics Specialists Conference*, San Francisco, California, USA, 1994.

[41] J. Alotaibi and R. M. Morales, "Efficient implementation of a helicopter hingless rotor model with active trailing edge flaps for control design," in *Proceedings of UKACC 12th International Conference on Control*, Sheffield, UK, 2018.

[42] W. Johnson, *Rotorcraft Aeromechanics*. Cambridge University Press, 2013.

[43] J. Alotaibi and R. M. Morales, "Mixed-Sensitivity $\mathcal{H}_\infty$ On-Blade control." in *Proceedings of the 44th European Rotorcraft Forum*, Delft, The Netherlands, 2018.

[44] H. Yang, J. Alotaibi, and R. M. Morales, "Advanced On-Blade control for vibration reduction of the EC-145 helicopter: Robust principal components vs $\mathcal{H}_\infty$," in *Proceedings of the AIAA Science and Technology Forum and Exposition 2020*, Orlando, Florida, USA, 2020.

[45] M. Grant and S. Boyd, "CVX: Matlab software for disciplined convex programming, version 2.1," http://cvxr.com/cvx, Mar. 2014.